REVIEW

Check for updates

Nanoparticles and bioorthogonal chemistry joining forces for improved biomedical applications

Javier Idiago-López, †ab Eduardo Moreno-Antolín, †a Jesús M. de la Fuente ab and Raluca M. Fratila *ab

Bioorthogonal chemistry comprises chemical reactions that can take place inside complex biological environments, providing outstanding tools for the investigation and elucidation of biological processes. Its use in combination with nanotechnology can lead to further developments in diverse areas of biomedicine, such as molecular bioimaging, targeted delivery, *in situ* drug activation, study of cell–nanomaterial interactions, biosensing, *etc*. Here, we summarise the recent efforts to bring together the unique properties of nanoparticles and the remarkable features of bioorthogonal reactions to create a toolbox of new or improved biomedical applications. We show how, by joining forces, bioorthogonal chemistry and nanotechnology can overcome some of the key current limitations in the field of nanomedicine, providing better, faster and more sensitive nanoparticle-based bioimaging and biosensing techniques, as well as therapeutic nanoplatforms with superior efficacy.

1. Introduction

Nanoparticles (NPs) have outstanding physical and chemical properties that have been exploited over the last decades in the biomedical field in the quest for advanced tools for the diagnosis and therapy of various diseases. Some of their unique optical and magnetic features at the nanoscale enable their use in detection/biosensing,[1] photodynamic therapy or magnetic and optical hyperthermia,[2,3] or as contrast agents in fluorescence, magnetic resonance, photoacoustic or photoluminescence imaging.[1,4] Additionally, suitably engineered NPs (for example liposomes, polymeric or mesoporous NPs) can act as nanocarriers for controlled delivery of therapeutic (bio) molecules,[2] providing several advantages over conventional systemic drug delivery, such as high loading capacity, cargo protection, improved drug pharmacokinetics, biodistribution and bioavailability and controlled release of the cargo (often based on the stimuli-responsiveness of the nanocarrier itself). Besides the use of their intrinsic physicochemical properties, many biological and biomedical applications of NPs rely on their coupling to other molecules, a process known as bioconjugation. The functionalisation of nanoparticles with relevant biomolecules (antibodies, aptamers, peptides, carbohydrates, *etc.*) can improve their ability to cross biological barriers and enables specific recognition of cell surface

receptors[5,6] (active targeting, as opposed to passive accumulation of NPs in solid tumours through the enhanced permeation and retention -EPR- effect[7]). It is very often that both diagnostic and therapeutic functions can be integrated in the same multifunctional nanoplatform, concept known as theragnosis.[8] Moreover, for specific applications (for example, signal amplification for detection or targeted drug delivery purposes), the use of multivalent nanoconjugates with high avidity (high density display of biomolecules on the nanoparticle surface) can be particularly advantageous.[9–11]

Over the past decade, an increasing number of publications reported biomedical applications of nanoparticles based on the use of bioorthogonal chemistries – reactions that can take place in complex environments, including living systems, with complete specificity and minimal interference with native biological processes.[12–15] Usually, a bioorthogonal reaction involves the incorporation of a chemical bioorthogonal reporter (see Section 2.2) to the target biomolecule by using the cell's own biosynthetic and metabolic mechanisms, followed by covalent reaction with an exogenous probe. However, performing bioorthogonal chemistry *in vitro* and *in vivo* is not a trivial task, for several reasons. First, not any chemical motif can function as a bioorthogonal reporter; in fact, only a handful of them are truly bioorthogonal (meaning that they do not interfere with biological functionalities) and possess selective reactivity toward their bioorthogonal partner. Second, bioorthogonal reactions must fulfil several stringent requirements, most of which are common to the so-called "click" reactions.[16] They must be water-compatible, not susceptible to the nucleophilic attack of ubiquitous amine and thiol groups present in biomolecules, not sensitive to redox and enzymatic chemistry,

aInstituto de Nanociencia y Materiales de Aragón (INMA), CSIC-Universidad de Zaragoza, Zaragoza 50009, Spain. E-mail: rfratila@unizar.es; javidlo@unizar.es; edmoreno@unizar.es; jmfuente@unizar.es

bCentro de Investigación Biomédica en Red de Bioingeniería, Biomateriales y Nanomedicina (CIBER-BBN), Spain

† Equal contribution.

and must not require heating above 37 °C, pressure or the presence of cytotoxic reagents and/or catalysts. Furthermore, they must be highly selective and have favourable reaction kinetics, given the low concentrations in which many biomolecules are present inside living systems. To date, diverse bioorthogonal reactions have proved their usefulness in many fields, such as biology, medicine, biomaterials science and nanotechnology. Examples include *in vitro* and *in vivo* imaging of biomolecules (antibodies, enzymes, glycans, *etc.*),[17–19] exosome[20,21] and cell[22,23] tracking, nuclear medicine,[24,25] manipulation of protein activity,[26] artificial cell–cell interactions,[27,28] *in vivo* tumour targeting,[29,30] prodrug activation,[31,32] nanosensing,[33] functionalisation of nanomaterials[29,34–39] and biomaterials.[40,41]

While plenty of reviews can be found in the literature on the topics of biomedical applications of NPs and on bioorthogonal

From left to right : **Javier Idiago-López**, **Jesús M. de la Fuente**, **Raluca M. Fratila** and **Eduardo Moreno-Antolín**

Javier Idiago and Eduardo Moreno are currently pursuing their PhD under the supervision of Prof Jesús M. de la Fuente and Dr Raluca M. Fratila at Instituto de Nanociencia y Materiales de Aragón (INMA, CSIC-University of Zaragoza). Javier's research uses bioorthogonal chemistry for the covalent immobilization of magnetic nanoparticles (MNPs) on cell membranes for magnetic hyperthermia applications. Eduardo works on the development of magnetoliposomes as cell membrane models to study the effect of the localised heating produced by the MNPs.

Jesús M. de la Fuente finished his PhD in 2003 (CSIC, Seville, Spain). In 2007, he obtained a permanent position at the University of Zaragoza to lead the Group of Biofunctionalization of Nanoparticles and Surfaces (Bionanosurf). He is currently Research Professor at INMA. His main research lines are focused on the use of nanotechnologies for advanced therapies and on the development of new transduction systems for biosensors.

Raluca M. Fratila obtained her PhD in 2005 (UPB, Bucharest, Romania). She joined the Bionanosurf group in 2013 and she is currently a Ramón y Cajal researcher at INMA. Her main research interests include bioorthogonal chemistry applied to nanomaterials, magnetic hyperthermia and biofunctionalisation of nanoparticles for biomedical applications.

chemistry separately, not so many are available concerning biomedical applications involving both bioorthogonal chemistry and nanotechnology. In our view, this is a field which will continue to expand in the coming years and will have a particularly strong impact in the development of new or improved biomedical applications. Therefore, in this review we present our vision on the unique opportunities that the powerful combination of bioorthogonal chemistry and nanotechnology can provide for bioimaging, biosensing/detection and therapeutic applications. We start by introducing some important concepts related to bioorthogonal chemistry, focusing on the main types of bioorthogonal reporters and bioorthogonal reactions discussed throughout the review (Section 2). We then turn our attention to the most promising applications in different areas, highlighting relevant examples from the fields of bioimaging, biosensing/detection and therapy (Section 3). For the sake of clarity and focus, we have curated a selection of representative examples that present clear *in vitro* and *in vivo* applications. We apologise in advance for any omission, and we encourage the reader to check Table 1, in which a more comprehensive compilation of references is included. Regarding the biomedical applications herein described, they are based on three main combinations of NPs and bioorthogonal reactions (Fig. 1):

(a) "Classical" bioorthogonal *in vitro* and *in vivo* coupling of NPs to cells or tissues – in these cases, the living systems are modified to incorporate chemical reporters and the NPs are suitably functionalised with the bioorthogonal partner.

(b) Bioorthogonal reactions taking place inside living systems between two building blocks, at least one of them being a nanoparticle; they do not necessarily involve a classical labelling of a living system with a bioorthogonal reporter, as in the first case. Note that, in some cases, bioorthogonal reactions falling into this category can be bond-breaking and not bond-forming reactions (bioorthogonal uncaging, see Section 3.6).

(c) Bioorthogonal chemistry approaches for NP functionalisation in view of the biomedical application. A comprehensive overview of the use of bioorthogonal chemistry for functionalisation of nanomaterials and nanoparticles is beyond the scope of this review; therefore, we only selected examples which are relevant in light of the biomedical applications of the corresponding NPs and we encourage the reader to consult detailed reviews on the topic.[29,33,36,42,43]

We hope that the examples discussed in this review will showcase the potential of bioorthogonal chemistry to address the following key issues in the field of biomedical applications of nanoparticles:

● Can bioorthogonal chemistry help in the development of more powerful NP-based bioimaging and biosensing techniques?

● Is it possible to improve the targeting abilities of NPs, going beyond classical passive (EPR effect) and active (receptor-based) targeting approaches?

● Can the combination of nanoparticles with bioorthogonal chemistry overcome some of the current translational hurdles in cancer nanomedicine (such as tumour heterogeneity)?

Table 1 Biomedical applications based on the combined use of bioorthogonal chemistry and nanoparticles. (a), (b) and (c) denote the type of bioorthogonal reaction as depicted in Fig. 1. The examples discussed more in detail in this review are marked with an asterisk

Reaction type	Reaction partners	Nanoparticle type	Biomedical application		Ref.	Year
Staudinger ligation	Azide + triarylphosphine	Polymer micelles	*In vivo* active tumour targeting[a]		49	2019
Copper-catalyzed alkyne–azide cycloaddition (CuAAC)	Azide + linear alkyne	Polymer dots	*In vitro* protein and glycoprotein labelling[a,*]		93	2010
		Magnetic mesoporous silica nanoparticles	Selective recognition and labelling of bacteria[a]		101	2016
		Carbon quantum dots	*In vitro* specific nucleus bioimaging[c,*]		102	2017
		Magnetic nanoparticles	*In vitro* cancer cell targeting[c]		103	2018
		Fluorescent nanodiamonds	*In vitro* imaging and tracking of membrane proteins[a,*]		92	2019
Strain-promoted alkyne–azide cycloaddition (SPAAC)	Azide + strained (cyclic) alkyne	Quantum dots	*In vitro* metabolic imaging[a,*]		69	2010
			In vivo imaging of respiratory viral infection[c]		104	2014
		Liposomes	*In vivo* tumour targeting and delivery[a,*]		105	2012
		Magnetic nanoparticles	*In vivo* pretargeted positron emission tomography imaging[b,*]		106	2013
			In vivo T_2 signal enhancement in MRI[c,*]		107	2014
		Glycol chitosan nanoparticles	*In vivo* active tumour targeting and drug delivery[a,*]		108	2014
			In vivo active tumour targeting[a,*]		109	2017
		Silica nanoparticles	Imaging of cellular localization and excretion of nanoparticles[b]		110	2015
		Gold nanoparticles	*In vitro* SERS imaging[c,*]		111	2017
		Glycol chitosan nanoparticles, gold nanoparticles, magnetic nanoparticles	*In vivo* stem cell tracking and imaging[a,*]		23	2017
		Dendrimer-based nanoparticles	*In vivo* active tumour targeting[a,*]		112	2017
			In vivo pretargeted nanoradioimmunotherapy[b]		113	2018
		Lipid nanoparticles	*In vivo* synergistic imaging-guided photothermal/photoacoustic therapy[a,*]		76	2017
		Mesoporous silica nanoparticles	*In vitro* pretargeting for enhanced diagnostic and therapeutic effect[b]		114	2018
		Biomimetic (T cell membrane-coated) polymeric nanoparticles	*In vivo* enhanced photothermal therapy[a]		94	2019
		Hybrid glycol chitosan – magnetic nanoparticles	*In vivo* imaging and tracking of stem cells in stroke[a,*]		115	2019
Strain-promoted alkyne-nitrone cycloaddition (SPANC)	Nitrone + strained (cyclic) alkyne	Magnetic nanoparticles	*In vitro* targeting[c]		34	2012
Inverse electron-demand Diels–Alder (IEDDA) reaction	Tetrazine + strained alkene/alkyne	Quantum dots	*In vitro* targeting[a]		55	2010
			In vivo single-cell multiplexed cytometric imaging[c]		116	2015
		Magnetic nanoparticles	Signal amplification for:	Biomarker detection[a,*]	95	2010
				Point-of-care micro-NMR for cancer diagnostics[a,*]	117	2011
				Intracellular biomarker detection[a]	96	2011
				Bacterial detection[a,*]	118	2011
				Detection of circulant tumour cells[a,*]	119	2012
				Tumour biomarker profiling[a,*]	97	2012
				Detection of glioblastoma-shed microvesicles for therapy monitoring[a,*]	120	2012
				Spatiotemporal labelling of cells with photoactivatable fluorophores[a]	121	2013
			Sequential prodrug activation[b,*]		122	2017
			In vitro cancer cell targeting[c]		103	2018
		Liposomes	*In vivo* pretargeted positron emission tomography imaging[b]		123	2013

Table 1   (Contd.)

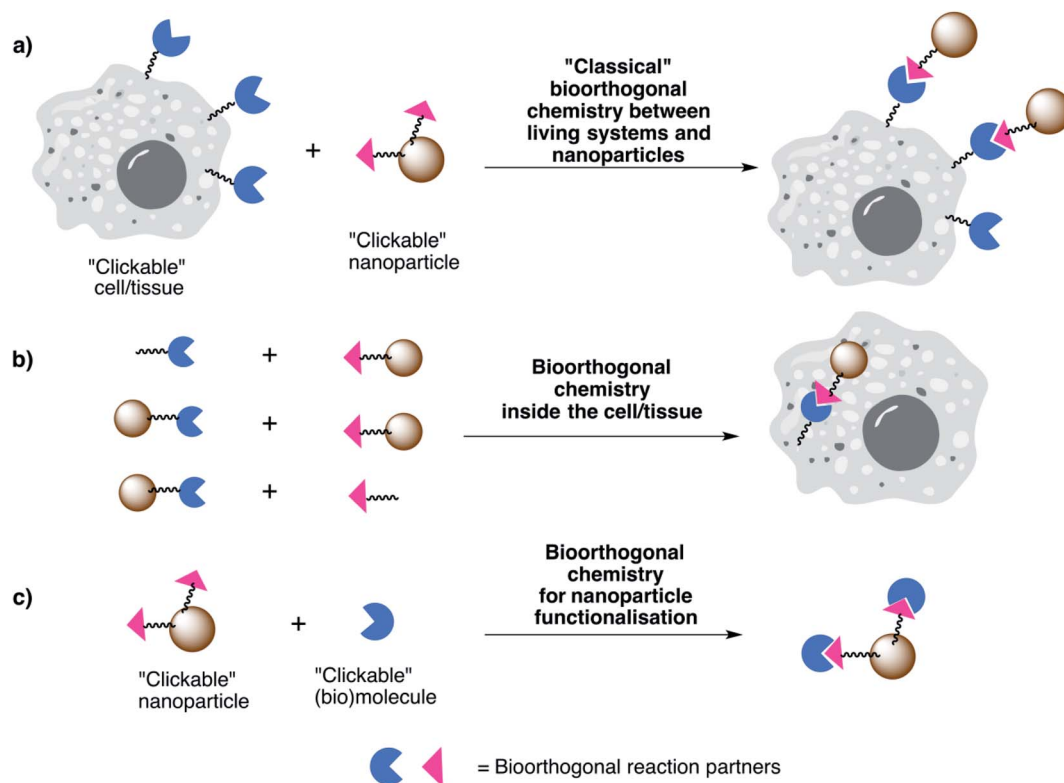| Reaction type	Reaction partners	Nanoparticle type	Biomedical application	Ref.	Year
		Albumin nanoparticles	*In vitro* intracellular drug delivery[a],*	91	2014
				100	2020
			In vivo intracellular drug delivery for enhanced therapeutic efficacy[a],*	98	2016
			In vivo enhanced photothermal therapy[a],*	124	2018
		Supramolecular, self-assembled nanoparticles	*In vivo* pretargeted positron emission tomography imaging[b],*	125	2016
		Mesoporous silica nanoparticles	*In vivo* pretargeted positron emission tomography imaging[b]	126	2017
			Tumour targeting[a],*	99	2019
		Hybrid ^{68}Ga-magnetic nanoparticles	*In vivo* pretargeted molecular imaging of atherosclerosis[b],*	127	2019
			In vivo fast pretargeted imaging of thrombi[b],*	128	2020
		Upconversion nanoparticles	"On" and "off" switching of photodynamic therapy function of nanoparticles *in vivo*[b]	129	2019
		Gold nanorods	*In vivo* prodrug activation, photothermal therapy and optoacoustic imaging[b],*	130	2019
		Polymeric nanostars	*In vivo* pretargeted positron emission tomography imaging[b],*	131	2020
		Carbon nanotubes	*In vivo* pretargeted fluorescence imaging[b],*	132	2020
		Nanomicelles	*In vivo* prodrug activation[b],*	133	2020
		Polymer brushes	*In vivo* pretargeted nuclear imaging[b]	134	2020
Oxime ligation	Oxyamine + aldehyde/ketone	Polymeric nanoparticles	*In vivo* active tumour targeting[a]	135	2015
		Liposomes	Cell transfection[a]	136	2017
Strain-promoted iminosydnone-cycloalkyne cycloaddition (SPICC)	Iminosydnone + strained alkyne	Nanomicelles	*In vivo* controlled release[b],*	137	2019

Fig. 1   Main types of combinations of NPs and bioorthogonal reactions discussed in this review.
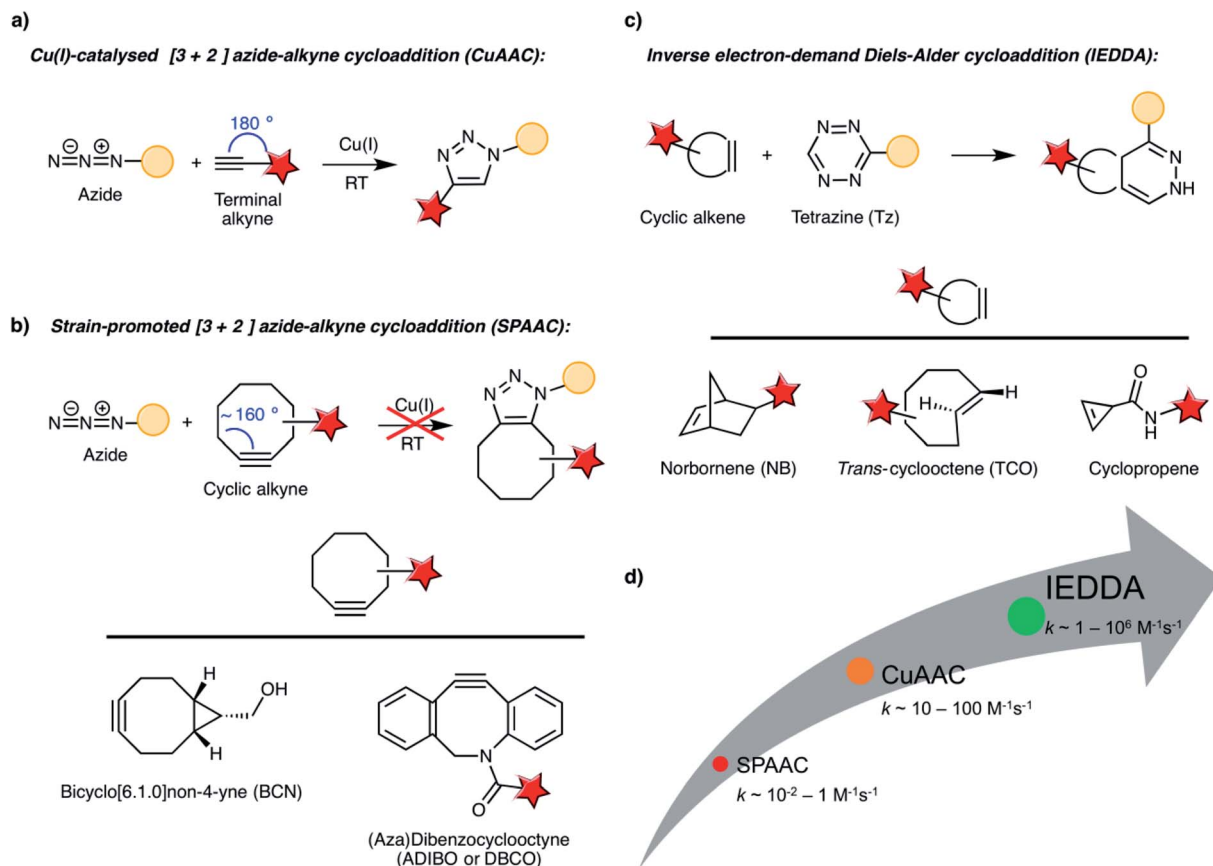
Fig. 2 (a–c) Main bioorthogonal reaction schemes discussed in this review, including representative examples of strained alkynes and cyclic alkene reagents. (d) Comparison of reaction kinetics of CuAAC, SPAAC and IEDDA.

2. Bioorthogonal chemistries – meet the partners

From a historical point of view, the "bioorthogonal chemistry revolution" started with the development of the Staudinger–Bertozzi ligation, based on the reaction between azides and tryarylphosphines.[44] The Staudinger–Bertozzi ligation has found several applications in chemical biology, including *in vivo* labelling of biomolecules in mice and zebrafish,[45,46] and recently the first examples of its use for the functionalisation of gold nanoparticles were reported by Workentin and co-workers.[47,48] However, it proceeds at slower rates than other bioorthogonal reactions and the phosphine reagents are prone to air oxidation, these probably being the reasons that prevent its more widespread use in nano(bio)technology. To the best of our knowledge, the first example of *in vitro* and *in vivo* applications involving nanomaterials and Staudinger ligation has been only recently described in the context of targeted delivery of polymer nanomedicines.[49]

In Section 2.1 we will turn our attention towards those bioorthogonal chemistry reactions that were most commonly used in the realm of nanotechnology, namely the azide–alkyne cycloadditions (in their copper-catalysed and strain-promoted versions, CuAAC and SPAAC, respectively) and the inverse

electron-demand Diels–Alder (IEDDA) cycloaddition (these reaction schemes are depicted in Fig. 2; see Table 1 for a broader overview of literature examples involving these and other types of bioorthogonal chemistries used for biomedical applications in combination with nanoparticles). As the focus of the review is on the final applications of the nanoparticles rather than on the bioorthogonal reactions, we will only provide the amount of detail considered necessary for the understanding of the topic and we will direct the reader to other relevant literature reviews on each of these bioorthogonal reactions, where available. Then, in Section 2.2 we will give a succinct overview of the main types of chemical groups used as bioorthogonal reporters and how they can be incorporated into the desired biomolecules.

2.1 Bioorthogonal reaction schemes

2.1.1 Copper-catalysed azide–alkyne [3+2] cycloadditions (CuAAC). Azides can act as 1,3-dipoles and undergo [3+2] dipolar cycloadditions with dipolarophiles such as activated alkynes to yield stable 1,4- and 1,5-disubstituted triazole adducts. However, in its classical form firstly described by R. Huisgen in 1963 the azide–alkyne [3+2] cycloaddition requires elevated temperatures, which obviously prevents its applications to living systems. In the early 2000′s the groups of K. B.

Sharpless[50] and M. Meldal[51] independently discovered that the addition of catalytic amounts of Cu(I) significantly enhanced the rate of the cycloaddition, enabling it to proceed in a regioselective fashion (only the 1,4-disubstituted triazole is obtained, with practically quantitative yield) at room or physiological temperature and over a broad pH range. The CuAAC is known as the quintessential example of click reaction and has been applied to a wide variety of biomolecules and bioconjugates (nucleic acids, proteins, enzymes, glycans, virus particles).[12,52,53] In terms of NP functionalisation, the CuAAC reaction has been extensively used for gold, polymeric, magnetic and carbon NPs;[29,36,54] however, it cannot be applied to typical, semiconductor nanocrystal-based quantum dots due to the fact that the Cu(I) catalyst quenches their fluorescence in an irreversible manner.[55] The primary drawback of the *in vitro/in vivo* CuAAC reaction is the necessity to employ the copper catalyst, which can lead to cytotoxic effects arising from the production of reactive oxygen species.[56–58] To tackle this problem, several groups designed more biocompatible Cu(I) catalysts based on ligand–copper complexes, which have been successfully employed for the labelling of different live mammalian cells as well as zebrafish embryos.[59–61] A special mention here goes to the development of nanoparticle-based copper catalysts, suitable for intracellular applications such as *in situ* drug synthesis.[58,62]

2.1.2 Strain-promoted azide–alkyne [3+2] cycloadditions (SPAAC). To overcome the cytotoxicity of the copper catalyst, the group of C. Bertozzi pioneered an alternative, copper-free azide–alkyne [3+2] cycloaddition in which the alkyne partner is constrained within an eight-membered ring (strain-promoted azide–alkyne [3+2] cycloaddition, SPAAC, Fig. 2b).[63] This geometry produces approximately 18 kcal mol^{-1} of strain, which leads to a dramatic increase in the reaction rate when compared to linear alkynes. However, SPAAC reactions involving simple cyclooctynes are rather slow (their second-order rate constants have values comparable to the Staudinger ligation, of 10^{-3} M^{-1} s^{-1}). Thus, much effort has been devoted towards the development of new families of more reactive cyclooctynes,[64–66] achieving up to 400 times faster kinetics with the biarylazacyclooctynone derivative BARAC ($k = 0.96$ M^{-1} s^{-1}).[67] Typical solutions for improving the reactivity of cyclooctynes include introducing electron-withdrawing groups such as fluorine[68,69] or additional strain elements, for example a cyclopropane ring opposite to the triple bond, leading to a bicyclo[6.1.0]non-4-yne (BCN) structure[70] and fused azadibenzocyclooctyne (ADIBO or DBCO) scaffolds.[67,71–73] It should be noted though that the increase in reactivity often comes at the expense of lower stability and shelf life, increased hydrophobicity and cumbersome and low-yield synthetic procedures. Therefore, a compromise must be sought for finding the best cyclooctyne derivative for each intended application. The functionalisation of nanoparticles with strained alkynes in view of *in vitro* and *in vivo* bioorthogonal reactions can be a particularly demanding issue. The chemistry employed to link the strained alkyne to the nanoparticle must not alter the stability and functionality/reactivity of neither the NP nor the alkyne (the reaction used for functionalisation of

nanoparticles with strained alkynes is in most cases the straightforward amide-bond formation). Some of the most reactive cyclooctynes are often not the ideal choice due to their hydrophobicity, which can affect the colloidal stability of the nanoparticles, especially at high-density modification of the NP surface. To overcome this issue, the strained alkyne can be modified to incorporate short ethylene glycol linkers[39,74] or can be linked to the polymer used to transfer to aqueous phase NPs that were synthesised in organic media;[75] another common strategy is the incorporation of polyethylene glycol (PEG) chains on the surface of the nanoparticle, often both as stabilizers and as functional linker to which the cyclooctyne can be conjugated.[69,76] Moreover, attention should be paid to the presentation and possible steric hindrance of the cyclooctyne moieties on the surface of the nanomaterial, in order to ensure the success of the SPAAC reaction with the azide-labelled biomolecule.

2.1.3 Inverse electron-demand Diels–Alder (IEDDA) reaction. The inverse electron-demand Diels–Alder (IEDDA) cycloaddition, developed in 2008 by the groups of Fox[77] and Weissleder,[78] is the fastest bioorthogonal click reaction reported so far, with kinetics of up to 10^6 M^{-1} s^{-1}.[79] The reaction takes place between an electron-deficient diene and a dienophile and, unlike the normal electron-demand Diels–Alder cycloaddition, it is irreversible. Typically, the role of the diene is played by 1,2,4,5-tetrazine (Tz) – and therefore this type of bioorthogonal reaction can be found sometimes in the literature as "tetrazine ligation" – while the dienophile partner is usually a *trans*-cyclooctene (TCO) or a norbornene (NB) derivative, although other dienophiles such as cyclopropene or cyclooctyne derivatives (*e.g.* BCN, DBCO) can be employed. IEDDA bioorthogonal chemistry is nowadays commonly used in chemical biology, imaging and materials science. This widespread use was made possible by the efforts put in the development of more robust and reactive tetrazines and dienophiles (for reviews highlighting synthetic advances in the field, see the excellent works of Oliveira *et al.*[25] and Wu and Devaraj[80]); however, what makes the IEDDA reaction truly outstanding for bioorthogonal applications is its ultrafast rate. This means that the IEDDA reaction can take place efficiently on biological time scales and at low concentrations, similar to those of many relevant biomolecules. As in the case of the SPAAC reaction though, several factors should be taken into account when conjugating IEDDA-reactive molecules to nanoparticles: reactivity, display of the diene or dienophile on the NP surface, stability and solubility of the molecule in aqueous media and colloidal stability of the final conjugate. Most of the examples found in the literature report the functionalisation of NPs with tetrazine derivatives, either directly to the NP coating (mostly *via* amide bond formation) or attached to PEG-type linkers for increased colloidal stability and avoidance of unspecific binding to cells. In general, unsubstituted tetrazine has faster kinetics, but is less stable in complex media such as serum, while tetrazines bearing electron-withdrawing groups are more reactive than those substituted with electron-donating groups, but show lower stability.[81]

2.2 Bioorthogonal reporters

The first step of a classical bioorthogonal "click" labelling as the one depicted in Fig. 1a involves the incorporation of a chemical reporter into the living system, ideally without significant structural alterations of the target biomolecule. This can be accomplished by using small, preferably abiotic chemical functionalities linked to substrates that can be used by the cell's own biosynthetic machinery. To date, several bioorthogonal reporters have demonstrated their usefulness for selective labelling of biomolecules, including aldehydes/ketones, azides, alkenes and alkynes, nitrones, thiols, tetrazoles, *etc.*[12,52,82,83] Most of the examples discussed in this review rely on the use of azides, (strained) alkenes and alkynes; the common pathways to incorporate these motifs into biomolecules are briefly discussed below.

2.2.1 Azides. Unnatural or noncanonical amino acids bearing azide groups can be incorporated into proteins either in a site-specific or a residue-specific fashion using the cell's translational machinery (this process is known as bioorthogonal noncanonical amino acid tagging – BONCAT – and can be applied for the generation of other bioorthogonal reporters, *vide infra*).[68,84–86] The installation of azide groups on glycans and glycoconjugates is typically achieved *via* metabolic glycoengineering, exploiting the fact that the sialic acid biosynthetic pathway is permissive of unnatural *N*-acyl monosaccharides. Following this approach, *N*-azidoacetylsialic acid (SiaNAz) and *N*-azidoacetylmannosamine (ManNAz) can be incorporated into cell's glycocalyx as *N*-azidoacetyl sialic acid,[44,87,88] *N*-azidoacetylglucosamine (GlcNAz) can be installed on cytosolic and nuclear proteins,[89] while *N*-azidoacetylgalactosamine (GalNAz) can be used for labelling mucin-type O-linked glycoproteins.[90] Metabolic glycoengineering is by far the most exploited strategy to decorate cells with bioorthogonal azide reporters, while a less conventional method includes the use of azide-modified antibodies.[91,92]

2.2.2 Alkynes. Typically, linear alkyne groups are generated using the BONCAT strategy described above, using alkyne-modified aminoacids such as homopropargylglycine,[93] while the incorporation of strained alkynes can be accomplished by metabolic glycoengineering with unnatural sugars bearing cyclooctyne moieties.[94]

2.2.3 Alkenes. Strained alkenes, the most popular alkene bioorthogonal reporters, are commonly introduced *in vitro* or *in vivo* by using suitably modified antibodies that recognize specific receptors.[95–100] The number of reactive cycloalkene groups linked to the antibody can be controlled by varying the concentration of cycloalkene reagent used and depends on the availability of reaction sites (typically, primary amines) of each antibody.

3. Biomedical applications based on nanoparticles and bioorthogonal reactions

In this section, we will discuss relevant examples of *in vitro* and *in vivo* biomedical applications of different types of NPs used in combination with bioorthogonal reactions. We will focus on several areas of relevance for diagnostic and therapeutic purposes, such as bioimaging (including the development of more sensitive imaging tools, stem cell tracking and pretargeted imaging), sensing (with emphasis on the bioorthogonal nano-amplification approach) and targeted therapeutic and/or theragnostic applications. The common thread throughout this section is the demonstration of how by leveraging the unique properties and characteristics of nanoparticles and bioorthogonal reactions, it is possible to advance these areas of research, leading to new or improved solutions to pressing issues such as sensitivity (in the case of imaging and sensing), tumour accumulation of nanoplatforms, maximised therapeutic efficiency, *etc.* At the beginning of each sub-section, we will provide a brief introduction to familiarise the reader with the particular field of application, its interest and specific challenges that need to be addressed.

3.1 Expanding the horizons of bioimaging applications

"Seeing is believing". This ancient proverb has become long time ago one of the paradigms of biomedicine. Visualising and monitoring biological processes at cellular and molecular scale can provide new insights into living systems and play a key role in the diagnosis and treatment of many diseases (*e.g.* cancer patient prognosis). Conventional approaches such as the use of organic fluorescent dyes or genetically encoded proteins have been used to track biomolecules in their natural milieu and to monitor cellular processes.[138,139] However, these probes can suffer from a lack of long-term photostability, intrinsic background signals generated because of the limited dye specificity or phototoxicity.[140,141] In addition, some of the fluorescent proteins are pH-sensitive and tend to oligomerise inducing non-fluorescent states.[142] On the other hand, although many imaging methods – computed tomography (CT), positron emission tomography (PET), magnetic resonance imaging (MRI), optical imaging, X-ray or ultrasound (US) – have been established in the medical field over the past few decades,[143,144] each of these modalities have their own drawbacks in terms of resolution, sensitivity, specificity or penetration depth. These issues can be alleviated by the use of nanotechnology, as the unique properties of certain nanoparticles make them ideal candidates for bioimaging applications.[1,4,145] These include high and long-term photostability, low toxicity or the possibility to combine diverse imaging techniques into a single, multi-modal nanoplatform.[4,146]

In this section, we will present some selected examples of *in vitro* and *in vivo* bioimaging in which the use of nanoparticles yields superior performance in terms of sensitivity and specificity when compared to conventional imaging probes.

Fluorescence imaging is one of the most powerful techniques for the analysis of dynamic information related with the concentration or localization of target (bio)molecules and requires the use of bright and photostable probes, especially for long-term studies. Inorganic semiconductor nanocrystals (quantum dots, QDots), having singular optical properties (tuneable and narrow emission spectra, good stability and long

photoluminescence lifetime), are ideal candidates for imaging applications. In one of the first examples of interfacing SPAAC with nanotechnology, Bernardin et al. reported the use of CdSe/ZnS QDots functionalised with a cyclooctynyl–glycolic acid derivative for imaging the metabolic incorporation of tetraacetylated N-azidoacetylmannosamine (Ac$_4$ManNAz) on the membranes of live Chinese hamster ovary (CHO) cells.[69] The strained alkyne was conjugated to the surface of amino-QDots via amide coupling and the reactivity of the resulting cyclooctynyl-QDots towards the bioorthogonal azide partner was tested both under CuAAC and SPAAC conditions. It has been shown that the use of Cu(I) can induce irreversible photoluminescence quenching via energy/electron transfer or alteration of the core structure of the QDots;[147] therefore, the fluorescence quantum yield of the conjugates obtained under Cu(I) catalysis was found to be about three times lower than the one of the corresponding SPAAC conjugates. In terms of bioorthogonal imaging capabilities, the QDots were used at nanomolar concentrations (organic dye probes typically require concentrations above 50 μM). The improved sensitivity over classical organic fluorophores was attributed to the multivalent presentation of the cyclooctyne groups on the QDot surface.

Despite the potential of QDots for bioimaging applications, they pose toxicity concerns related to the presence of heavy metal ions;[148] this led to the development of more biocompatible alternatives, such as polymer dots and carbon quantum dots. Semiconducting polymer dots (PDots) are non-toxic and exhibit superior properties when compared to QDots in term of brightness and photostability;[149] moreover, unlike QDots, they are compatible with the CuAAC reaction. However, achieving control over their surface (bio)functionalisation is not trivial and poses a considerable challenge for the use of PDots for biological applications. Chiu and co-workers addressed this difficult task by co-condensing a highly fluorescent semiconducting polymer (poly[(9,9-dioctylfluorenyl-2,7-diyl)-co-(1,4-benzo-{2,1′,3}-thiadiazole)] – PFBT) with an amphiphilic copolymer (poly(styrene-co-maleic anhydride) – PSMA).[93] The resulting PDots bearing carboxyl groups on their surface were further functionalised with propargylamine and used for the fluorescent labelling of newly synthesised proteins and O-linked glycoproteins in MCF-7 human breast cancer cells. The azide reporters were introduced into the target biomolecules following the bioorthogonal noncanonical amino acid tagging (BONCAT) strategy for proteins and the metabolic glycoengineering approach using GalNAz for glycoproteins, respectively. This work demonstrates the potential of PDots to function as ultrabright fluorescent nanoprobes for bioimaging applications with excellent sensitivity (nanomolar concentrations) and specificity (no background signal in the controls lacking the azide reporter). Carbon quantum dots (CQDots), discovered accidentally in 2004, have emerged as another non-toxic alternative to traditional QDots. Although the exact mechanism behind their photoluminescence is still not fully understood, it is thought that the different electronic states of carbon in the core–shell nanostructure of the CQDots (sp^2 in the core and sp^3 in the shell) are responsible for the absorption and emission features.[150] It is also assumed that the surface functionalisation
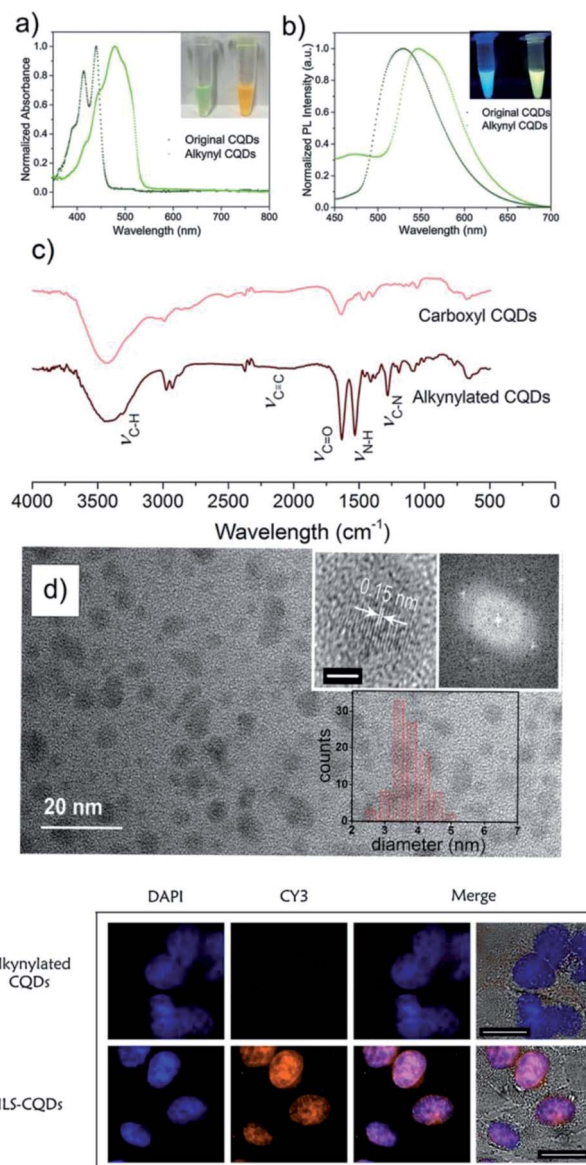

Fig. 3 Top: Photophysical properties of original (carboxyl)- and alkynyl CQDots: (a) absorption spectra, (b) photoluminescence spectra, (c) FTIR spectra, (d) TEM analysis of the alkynylated CQDots. Bottom: Confocal microscope images of HEp-2 cells incubated with alkynylated CQDots and NLS-CQDots, respectively, under DAPI channel (Hoechst 33258) and CY3 channel (CQDots). Scale bar: 10 μm. Reprinted from Chem.–Eur. J., 23, M. X. Gao et al., "Click" on alkynylated carbon quantum dots: an efficient surface functionalization for specific biosensing and bioimaging", 2171–2178, Copyright (2017), with permission from John Wiley & Sons Ltd.

of these nanomaterials plays a key role in tuning their photoluminescent properties, as their excitation/emission spectra shift as a consequence of electronic structure changes induced by surface modification.[151] Huang and co-workers reported for the first time the functionalisation of CQDots using CuAAC click chemistry for bioimaging applications (Fig. 3a–d),[102] following a strategy based on alkynylated CQDots (prepared from carboxyl-rich CQDots through amidation with propargylamine in the presence of 1,1′-carbonyldiimidazole), which
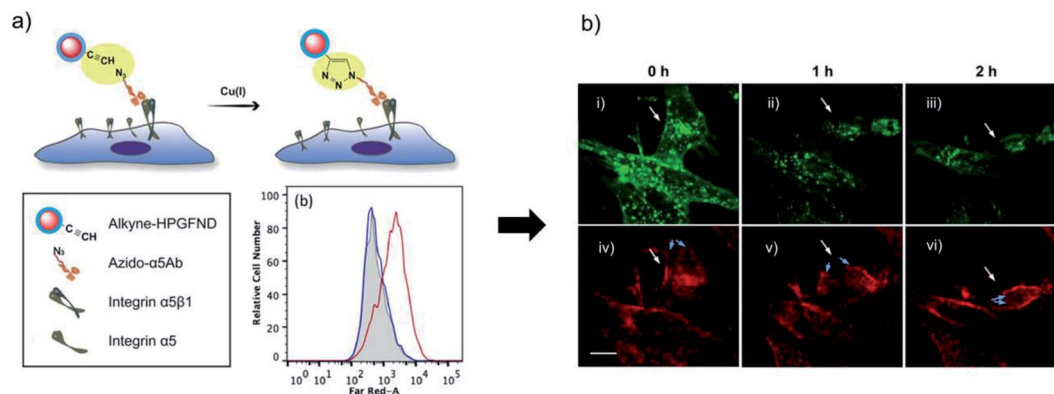
Fig. 4 Bioorthogonal labelling of integrin α5 membrane proteins using azide–modified antibodies and alkyne–HPGFNDs: (a) flow cytometry analysis of fluorescence signals from HFW cells preincubated with Azido-5αAb (red) and control cells (blue). (b) HFW cells labelled with Alexa Fluor 488-conjugated wheat germ agglutinin (i–iii) and 100 nm alkyne-HPGFNDs (iv–vi). White arrows indicate the cell migration route and blue arrows show the migration of integrin α5 on cells filopodia. Scale bars: 20 μm. Adapted with permission from ACS Appl. Mater. Interfaces, 11, Hsieh et al., "Bioorthogonal Fluorescent Nanodiamonds for Continuous Long-Term Imaging and Tracking of Membrane Proteins", 19774–19781. Copyright (2019) American Chemical Society.

underwent a CuAAC reaction with an azido-nuclear localisation sequence (NLS) peptide. *In vitro* fluorescence microscopy studies in human epidermis larynx carcinoma (HEp-2) cells demonstrated that the NLS-modified CQDots could act as efficient and specific nucleus imaging probes without any associated cytotoxicity.

As it has been mentioned previously, one of the main limitations of conventional techniques based on fluorescent dyes or genetically encoded proteins for bioimaging is their short-term photostability.[140,152] In this regard, Hsieh et al. described the use of alkyne-functionalised fluorescent nanodiamonds (FNDs) for the study of membrane protein dynamics in living cells over 10 hours.[92] Nanodiamonds are carbon nanoparticles with a diamond core (with sp^3 electronic configuration) coated by graphitic or amorphous carbon layers (with sp2 electronic configuration). This singular atomic structure provides them with unique optical, mechanical and magnetic properties.[153] Particularly, negatively charged nitrogen-vacancy centres provide them with bright red/near-infrared fluorescence and great photostability. The authors developed a one-pot method for the synthesis of biocompatible alkyne-functionalised hyperbranched-polyglycerol-coated FNDs (alkyne-HPGFNDs) with good colloidal stability in biological media. The nanodiamonds were attached *via* CuAAC to the surface of HFW cells (human fibroblasts) labelled with azide-modified antibodies against integrin α5 (Fig. 4a). Time lapse fluorescence images confirmed the high temporal and spatial imaging resolution of the target protein with a predefined reorganisation in cell migration route, with a time frame above the detection limits available for organic fluorophores (Fig. 4b).

The combination of nanoparticles and bioorthogonal reactions can be applied to other imaging modalities, besides fluorescence imaging. For instance, gold nanoparticles (AuNPs) exhibit a characteristic surface-enhanced Raman spectroscopy (SERS) signal that can be amplified by coupling Raman-active molecules.[154] SERS has emerged in recent years as a new

imaging tool, with potential for multiplex analysis *in vivo* either alone or in combination with other imaging techniques.[155] Liu et al. pioneered the use of SPAAC for the development of a folate receptor (FR) – targeted SERS nanoprobe.[111] The nanoprobe consisted of hollow gold nanoparticles (HAuNPs) coated with a Raman-active azide derivative (5,5′-dithiobis(2-nitrobenzoic acid)-N$_3$ (DNBA-N$_3$)) and then functionalised with folate-BCN *via* the copper-free click reaction (Fig. 5a). This particular nanosystem was reported to have high stability in cell culture medium, provided by the PEG chain present in the DNBA-N3 derivative, and a stable Raman shift at 1332 cm^{-1} (because of the nitro group stretch) for up to three months in aqueous conditions. The system was tested in three different cell lines (human nasopharyngeal epidermoid carcinoma – KB, cervical carcinoma – HeLa, and lung adenocarcinoma – A549) with different levels of expression of folic acid receptor. Dark field images and confocal Raman microscopy revealed a clear targeting and imaging of FR-positive cancer cells with high spatial resolution using a very low concentration of nanoprobe (50 pM) and without unspecific interactions. In particular, KB cells showed a much higher Raman signal in comparison with HeLa and A549, in accordance with the decrease of the FR expression levels, respectively (Fig. 5b and c). In addition, controls with unclicked HAuNPs and folic acid-free (FA-free) competition experiments revealed the high specificity of the imaging approach (Fig. 5b).

Iron oxide nanoparticles (IONPs) offer interesting properties for bioimaging due to their transversal T$_2$-relaxation signal in magnetic resonance imaging.[156] In an elegant approach, Gallo et al. reported the self-assembly of IONPs *via* SPAAC in the tumour environment, with the aim of improving the sensitivity of the MRI probe.[107] Two sets of IONPs, functionalised with azides (azido-polyethylene glycol) and strained alkynes (cyclooctynyl–glycolic acid derivatives), respectively, were used as SPAAC partners. To improve their tumour targeting capabilities, both sets of IONPs were also decorated with targeting peptides
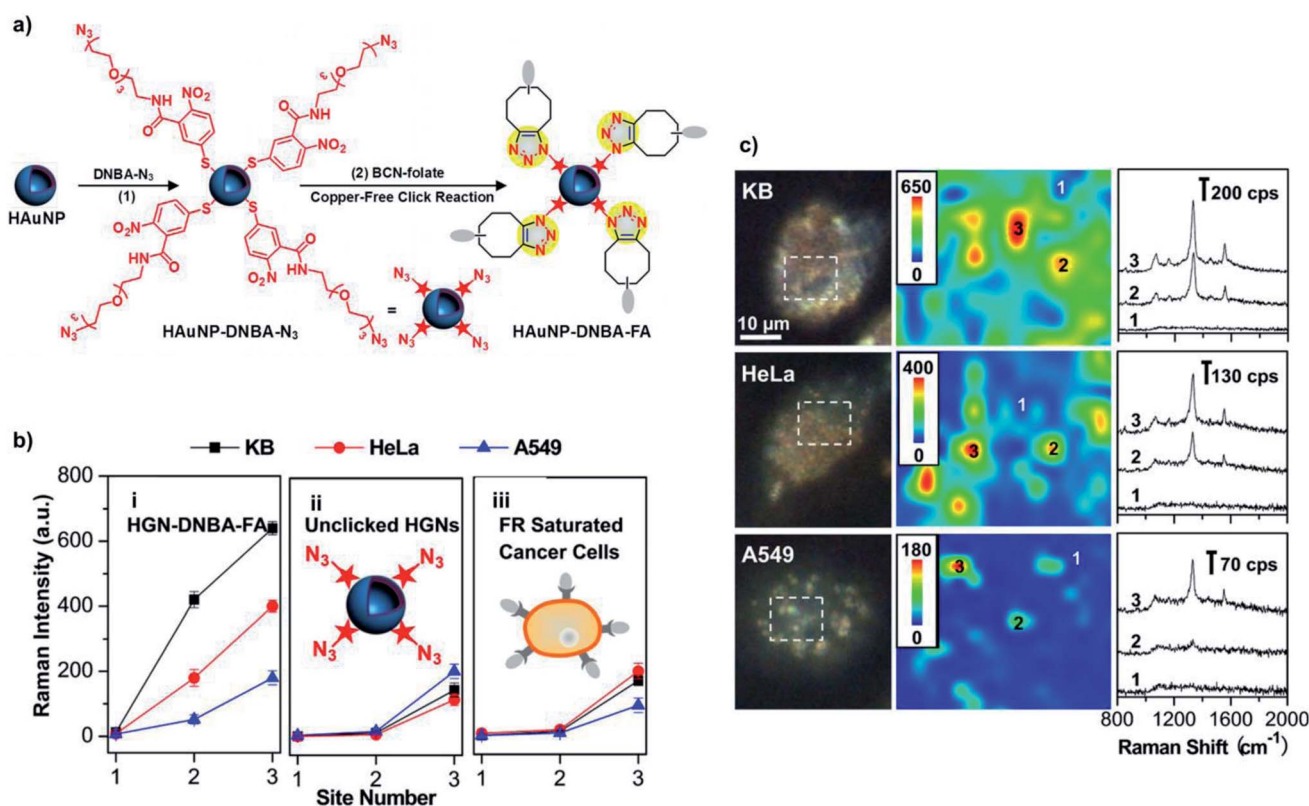
Fig. 5 (a) Workflow of the synthesis of folic acid functionalised SERS nanoprobes *via* SPAAC. (b) Raman intensities of 1332 cm^{-1} from KB, HeLa, and A549 at three local sites selected on each cell line and with three incubation conditions for 1 h: (i) HAuNP–DNBA–FA, (ii) unclicked HAuNP–DNBA–N$_3$, (iii) HAuNP–DNBA–FA in cells previously saturated with FA. (c) Dark field images of the three cell lines incubated with HAuNP–DNBA–FA nanoprobes (50 pM) for 1 h and the corresponding SERS images and Raman spectra. Adapted with permission from ACS Appl. Mater. Interfaces, 9, R. Liu *et al.*, "Click-functionalised SERS nanoprobes with improved labeling efficiency and capability for cancer cell imaging", 38222–38229. Copyright (2017) American Chemical Society.

for C–X–C chemokine receptor type 4 (CXCR4), which is over-expressed in metastatic tumours. Finally, the design of the nanoplatforms also included a peptide sequence cleavable by tumour metalloproteinases 2 and 9 (MMP2/9). *In vitro* studies in U87 glioblastoma cells expressing CXCR4 and MMP9 demonstrated that the cleavage of the MMP2/9 peptide sequence triggered the SPACC reaction between the two sets of IONPs and led to a T_2 signal enhancement of around 160% because of the nanoparticle self-assembly. Furthermore, intravenous injection in U87 tumour xenograft mice revealed a decrease of the T_2 relaxation time around 14% 4 h post-injection, while in the case of the control experiments performed with non-targetable IONPs no significant change in the tumour contrast was appreciated.

3.2. Stem cell imaging and tracking

The use of stem cells can provide new therapeutic approaches for the fields of regenerative medicine or cancer treatment.[157,158] The development of efficient and non-invasive imaging technologies for *in vivo* tracking of stem cells is crucial for their implementation in therapy. In this regard, a wide variety of nanoparticles (quantum dots, gold, polymeric and iron oxide magnetic nanoparticles) have been tested already for the

labelling of stem cells with imaging agents.[159] However, this approach is limited by the intrinsic low endocytic capability of stem cells, the heterogeneity in receptor-mediated nanoparticle uptake, the loss of signal intensity induced by cell proliferation or the potential side effects that certain nanomaterials can have on cell differentiation or viability.[159,160] The incorporation of artificial receptors on stem cell membranes *via* metabolic glycoengineering and the subsequent bioorthogonal click reaction with nanoparticles can enable a well-defined and homogeneous labelling of stem cells before *in vivo* implantation.

In one of the earliest approaches, Lee *et al.* developed a novel imaging system for *in vivo* tracking of transplanted stem cells based on bioorthogonal SPAAC chemistry.[23] For this purpose, bicyclo[6.1.0]non-4-yne (BCN) moieties were covalently attached *via* amide coupling onto the surface of glycol chitosan nanoparticles (CNPs) encapsulating different types of imaging agents – Cy5.5 cyanine dyes for fluorescence, iron oxide nanoparticles for MR and gold nanoparticles for CT imaging (Fig. 6a). The BCN-modified CNPs were subsequently efficiently linked to the surface of Ac$_4$ManNAz-treated adipose tissue-derived human mesenchymal stem cells (hMSCs) within only one hour of incubation. As proof-of-concept of the potential of this new labelling strategy, the resulting BCN–CNP-imaging agent-
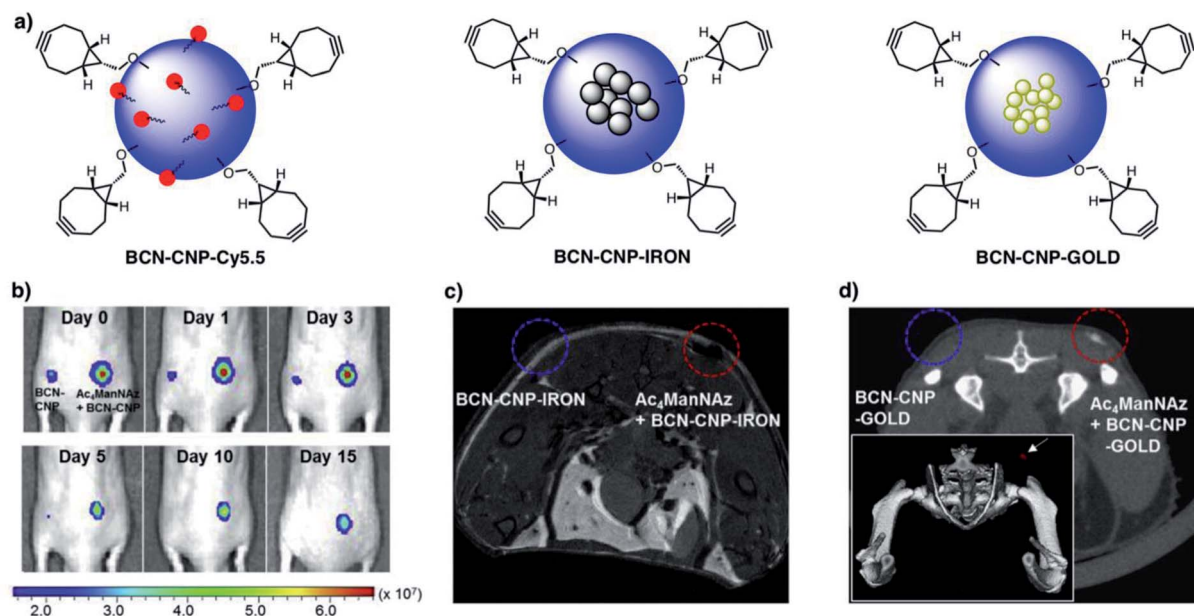
Fig. 6 BCN–modified glycol chitosan nanoparticles for cell stem labelling and imaging. Top: Schematic structures (a). Bottom: NIRF (b), T_2-weighted MRI (c) and micro CT (d) imaging of mice after transplantation of BCN–CNP-Cy5.5/IRON/GOLD labelled stem cells with and without Ac$_4$ManNAz pre-treatment. Adapted from Biomaterials, 139, S. Lee et al., "In vivo stem cell tracking with imageable nanoparticles that bind bioorthogonal chemical receptors on the stem cell surface", 12–29, Copyright (2017), with permission from Elsevier.

modified stem cells were transplanted into the dorsal subcutaneous region of nude mice and their in vivo fate was investigated by non-invasive imaging techniques. Labelled stem cells could be visualized up to 15 days post-transplantation by near-infrared fluorescence (NIRF) imaging, in contrast to cells lacking the Ac$_4$ManNAz pre-treatment, whose NIRF signal disappeared in 5 days (Fig. 6b) because of the taken-up effect by host normal cells and macrophages at the transplanted site in vivo. The transplanted stem cells could be also followed by MRI and micro CT imaging (Fig. 6c and d), demonstrating the usefulness of bioorthogonal SPAAC chemistry compared to non-specific nanoparticle uptake for stem cell tracking applications.

More recently, the same group reported a similar nanosystem based on BCN-conjugated glycol chitosan nanoparticles for dual-modal stem cell imaging in mouse brain stroke (BCN-dual-NPs).[115] These nanoparticles were conjugated with the NIRF probe mentioned in the previous example (Cy5.5), while 20 nm oleic acid-coated superparamagnetic iron oxide nanoparticles were encapsulated in their hydrophobic core for optimal T_2-MRI contrast. Prior to in vivo implantation of cells, the bioorthogonal labelling conditions were optimised in vitro with adipose-derived hMSCs (Fig. 7a). A low concentration of 10 μM Ac$_4$ManNAz was selected as optimal for the expression of azide membrane reporters without interfering with the cellular metabolic activity and viability. In addition, 300 μg mL^{-1} of BCN-CNPs rendered the highest SPAAC ligation in 2 h of incubation with minimal unspecific interaction in cells without Ac$_4$ManNAz treatment. Furthermore, cell proliferation and differentiation studies confirmed that the bioorthogonal labelling of hMSCs with BCN-dual-NPs did not induce changes in their phenotype, which is a key feature of an ideal stem cell

labelling method. After inducing photothrombotic stroke (PTS) in the brains of Balb/c nude mice, the migration of the bioorthogonally labelled hMSCs from the implantation site to the stroke lesion was monitored in real time for 14 days, both by NIRF and MRI. A gradual decrease of the respective NIRF and MRI signals at the implantation area was observed, with the concomitant increase in intensity at the stroke lesion, demonstrating the potential of this dual probe for non-invasive and real-time monitoring of stem cell fate with high spatiotemporal resolution.

3.3 Pretargeted imaging

Tumour pretargeted imaging is one of the fields where the combination of bioorthogonal chemistry and nanotechnology could have a tremendous impact in the next years, offering solutions to some of the problems currently associated with clinical imaging modalities, such as short half-lives of imaging probes or suboptimal accumulation in the tumours.[161] To date, several types of nanoparticles and nanomaterials have been explored for tumour pretargeted imaging purposes in combination with SPAAC or IEDDA click reactions, including mesoporous silica nanoparticles (MSNs),[106,126] polymeric nanostars,[131] supramolecular NPs,[125] carbon nanotubes,[132] or polypeptide-based polymer brushes.[134] Kim and co-workers introduced the MSN-based pretargeting using the SPAAC reaction between DBCO-modified MSNs and a short-lived ^{18}F-labeled azide for positron emission tomography imaging.[106] DBCO-MSNs injected intravenously into mice bearing subcutaneous U87 (glioblastoma) tumours accumulated in the tumour tissue due to the EPR effect and acted as pretargeting system (Fig. 8a). The PET radiotracer, which alone has no
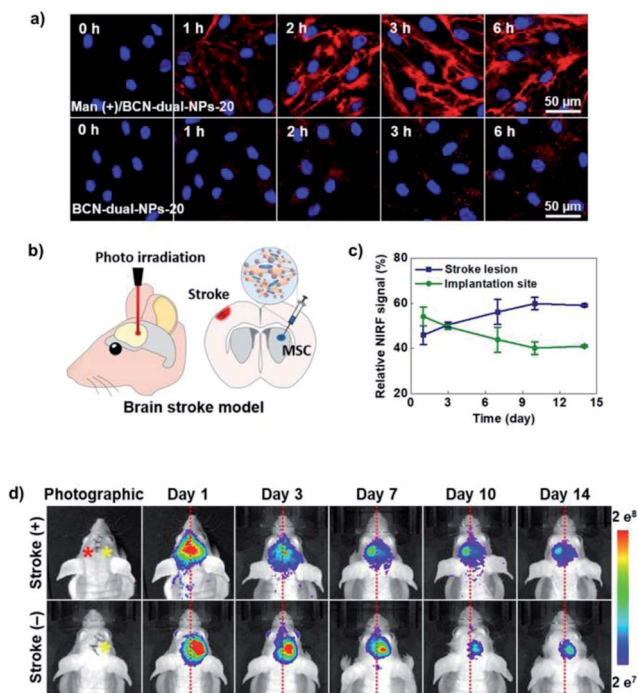
Fig. 7 (a) Confocal microscope images at different incubation times showing *in vitro* bioorthogonal labelling of hMSCs with BCN-dual-NPs-20 in Ac$_4$ManNAz pre-treatment conditions (Man (+)) and in control cells. (b) Scheme of brain stroke induction in mice and the hMSC implantation. (c) Relative NIRF signal between the stroke lesion (left brain) and bioorthogonally-labelled hMSC implantation site (right brain). (d) *In vivo* real-time tracking of bioorthogonally-labelled hMSCs in a mouse PTS model. Comparison of bioorthogonally-labelled hMSCs with BCN-dual-NPs-20 migration between stroke (+) and stroke (−) mice models by NIRF imaging during 14 days. The red and yellow asterisks indicate the stroke lesion and stem cell implantation site, respectively. Adapted with permission from ACS Nano, 13, S. Lim *et al.*, "Dual-modal imaging-guided precise tracking of bio-orthogonally labeled mesenchymal stem cells in mouse brain stroke", 10991–11007. Copyright (2019) American Chemical Society.

tumour targeting capability, was administered both to mice pre-treated with DBCO-MSNs and to control animals. PET imaging revealed that pretargeting with MSNs significantly enhanced the signal in the tumour up to two hours post-injection of the radiotracer (Fig. 8c). On the contrary, in control animals the PET tracer suffered a rapid renal clearance (Fig. 8b). The fast kinetics of the SPAAC reaction plays a crucial role in this example, due to the short half-life of the ^{18}F isotope (<120 min) and highlights the unique capabilities of bioorthogonal chemistry for real-time, non-invasive bioimaging applications.

Hou *et al.* described a tumour pretargeting imaging system based on the use of inverse electron-demand Diels–Alder reaction.[125] Supramolecular nanoparticles (SNPs) were synthesized *via* self-assembly of four different components (TCO-grafted cyclodextrin–polyethylenimine polymer, TCO/CD-PEI; cyclodextrin–polyethyleneimine polymer, CD-PEI; adamantane-grafted polyamidoamine, Ad-PAMAM; Ad-grafted polyethylene glycol, Ad-PEG) at well-defined concentrations to provide a fine control of the pharmacokinetics of the system. In addition, this

particular configuration with the encapsulated TCO-probe renders certain advantages in terms of overcoming the TCO hydrophobicity, increasing the local probe concentration or reducing its degradation during tumoral delivery. The supramolecular system was administered intravenously (100 μg, equivalent to 1 nmol of TCO) to mice bearing U87 glioblastoma xenografts and accumulated in the tumour by EPR effect; its disassembly was triggered by the lower pH environment of the tumour and enabled the reaction of the released TCO/CD-PEI with a tetrazine–radiolabelled probe (^{64}Cu–Tz, 100 μL, equivalent to 10 nmol of Tz, injected *via* tail vein 24 h after the injection of the SNPs). Two controls without pretargeting were also tested: a first one was based on the intravenous injection of free ^{64}Cu–Tz, while in the second one the ^{64}Cu–Tz tracer was reacted with TCO-SNPs prior to the injection. PET images and *ex vivo* radioactivity biodistribution analysis revealed a preferential accumulation of the radiolabelled probe (^{64}Cu) in the tumour for the pretargeted strategy, with 16% injected dose per gram of tissue detected in the tumour and with residual values in the case of the controls, which had their main signal located in the liver. It is worth mentioning that the accumulation of the radiotracer in the tumour was far superior in this work when compared to the previously discussed study by Kim and co-workers (16% *vs.* 1.3%); this could be attributed to the faster reaction rate of the IEDDA and to the TCO protection by the supramolecular nanoparticle system. Another approach based on the IEDDA reaction was reported by Goos and co-workers, who developed multivalent polymeric nanostars functionalised with TCO moieties either directly or by means of a short (PEG$_{12}$) or a long (PEG$_{106}$) PEG linker.[131] The nanostars accumulated passively in tumours with EPR characteristics, and were targeted with Tz-bearing fluorinated radiotracers. Interestingly, the distance between the TCO groups and the nanostar backbone was found to play a key role in the yield of the bioorthogonal reaction and dictated the tumour-to-tissue ratios, with the TCO conjugated directly to the nanostar architecture being the most reactive and the most efficient in terms of tumour accumulation of the tetrazine radiotracer. This effect was attributed to the steric hindrance that long PEG chains could exert, resulting in a loss of reactivity of the TCO moieties, and demonstrates the importance of a careful design of nanoparticles for *in vivo* bioorthogonal reactions. Finally, we wish to highlight a very recent example of the use of IEDDA chemistry for pretargeted tumour imaging, which makes use of carbon nanotubes (CNTs) rather than nanoparticles and of bioorthogonal bond cleavage instead of bond formation.[132] This novel strategy enabled for the first time a very precise spatio-temporal control of the activation of a fluorogenic NIR imaging probe only inside the tumour as a result of the bioorthogonal cleavage reaction. Mice bearing colon carcinoma-derived tumours were treated in a first step with Tz-modified single-walled carbon nanotubes (Tz-SWCNTs) and two hours later with a TCO-caged hemicyanine dye (tHCA, non-fluorescent), both *via* intravenous injection. The two-hours gap between the administration of the bioorthogonal partners was sufficient to enable the clearance of the Tz-SWCNTs from the blood and their EPR effect-mediated accumulation in the tumours. Three
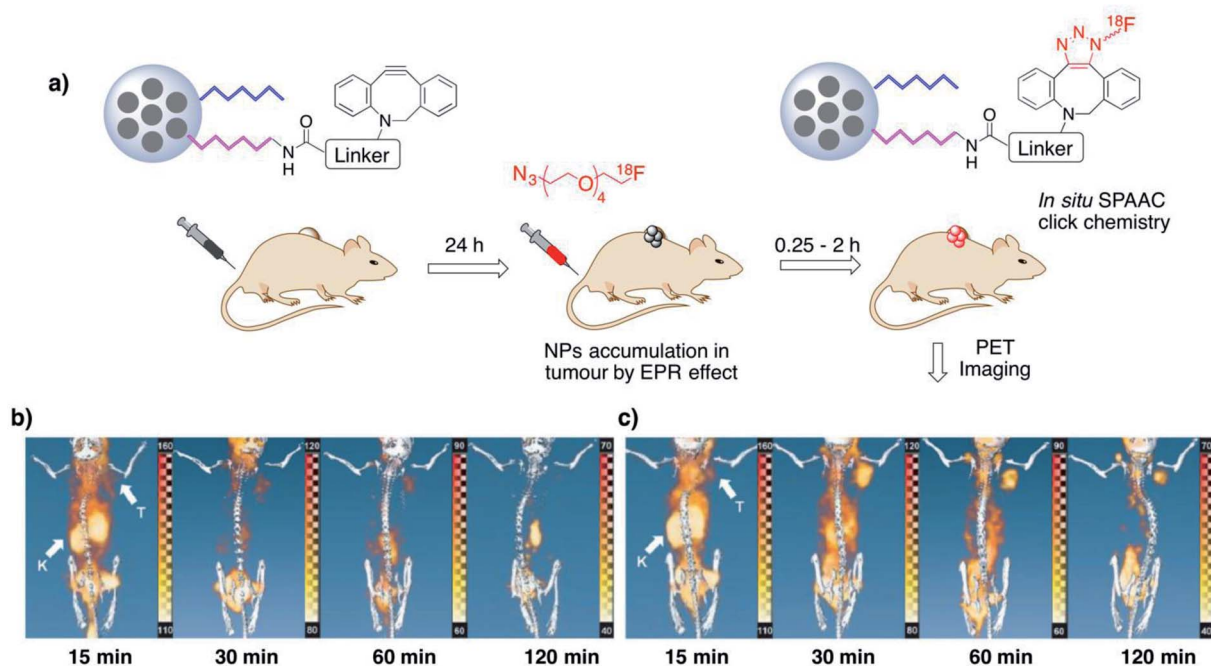
Fig. 8 Pretargeting approach using SPAAC click chemistry between DBCO–MSNs and azide–labelled radiotracers (a) and PET–CT imaging of mice bearing U87 tumours (b and c). Mice lacking the pretargeting treatment (control, b) showed rapid renal excretion of the radiotracer. In mice treated with DBCO–MSNs (c) a persistent PET signal in the tumour site could be observed up two 120 min post–injection of the tracer. White arrows indicate kidneys (K) and tumour (T). Adapted from Angew. Chem., Int. Ed., 52, S. Lee et al., "Mesoporous silica nanoparticle pretargeting for PET imaging based on a rapid bioorthogonal reaction in a living body", 10549–10552, Copyright (2013), with permission from John Wiley & Sons Ltd.

hours after the tHCA injection, a clear fluorescence signal started to appear in the tumour areas as a consequence of the HCA uncaging due to the IEDDA reaction between the TCO and the Tz-SWCNTs; a maximum tumour-to-background ratio was reached after 24 hours. By contrast, in mice treated with tHCA alone, only a faint fluorescence signal could be appreciated in the abdominal area 1.5 hours post-injection, disappearing after three hours. Interestingly, this two-steps strategy resulted better in terms of tumour selectivity than direct delivery of a classical Cy5.5 NIR fluorescent probe (administered as Tz-SWCNTs-Cy5.5).

The pretargeting strategy can be also applied to other disorders for which molecular imaging is crucial in the diagnosis, as in the case of atherosclerosis. Recently, Pellico et al. developed a bimodal PET-MRI detection system based on the use of nano-radiomaterials (NRMs) consisting of tetrazine-functionalised iron oxide nanoparticles loaded with ^{68}Ga isotopes (^{68}Ga-NRM-Tz) (Fig. 9a).[127] Oxidised low density lipoprotein (oxLDL), which plays a key role in the development of atherosclerosis, was used as a target for *trans*-cyclooctene labelled antibodies (Ab-TCO). *In vivo* experiments were carried out using Apolipoprotein E-deficient mice (ApoE–/–), which are well established animal models for atherosclerosis. The strategy followed was based on the intravenous injection of ^{68}Ga-NRM-Tz (1.7 nmol Tz, 1.4 mg Fe/mL) 24 h after the injection of Ab-TCO (55 pmol, Fig. 9b). Biodistribution and clearance assays of pretargeted NRMs were tested with a large accumulation in aorta and effective circulation clearance in 90 min without liver

function damage. Subsequently, the pretargeted approach was examined in four groups of mice: (i) ApoE-/- on high fat diet, (ii) ApoE-/- on normal diet, (iii) Control mice C57BL/6 and (iv) ApoE-/- on high fat diet but with NRMs without tetrazine. In addition, an extra group of mice previously injected with TCO-free antibody in order to block the NRM recognition sites was tested. *In vivo* PET images were recorded and aortas were analysed by *ex vivo* T_1-MRI. PET imaging of the aortic arch revealed a clear signal in the case of the mice belonging to group (i), while for the animals from the rest of groups the signal was negligible. Moreover, a radioactive analysis revealed an outstanding accumulation of the NRMs in the same group of mice with a 14.7 2.7% of injected dose per gram of tissue. Finally, magnetic resonance (MR) images comparing the aortas of mice ApoE-/- on high fat diet with ^{68}Ga-NRM-Tz and ^{68}Ga-NRM revealed a clear detection profile and probing the specificity of the bioorthogonal reaction and viability of the approach with short half-life radioisotopes and very low concentrations of Ab and NRM. Just as this manuscript was being finalised, Herranz and collaborators reported a new imaging application of a very similar system, named "thrombo-tag".[128] Here, a fast pretargeted imaging approach was applied, by mixing the two components of the bioorthogonal system (^{68}Ga-NRM-Tz and TCO-*anti*-CD41 antibody, targeting integrin alpha chain IIb on membrane of platelets) and co-injecting them in order to promote the accumulation of the probes and the IEDDA reaction to take place simultaneously. This is of outmost
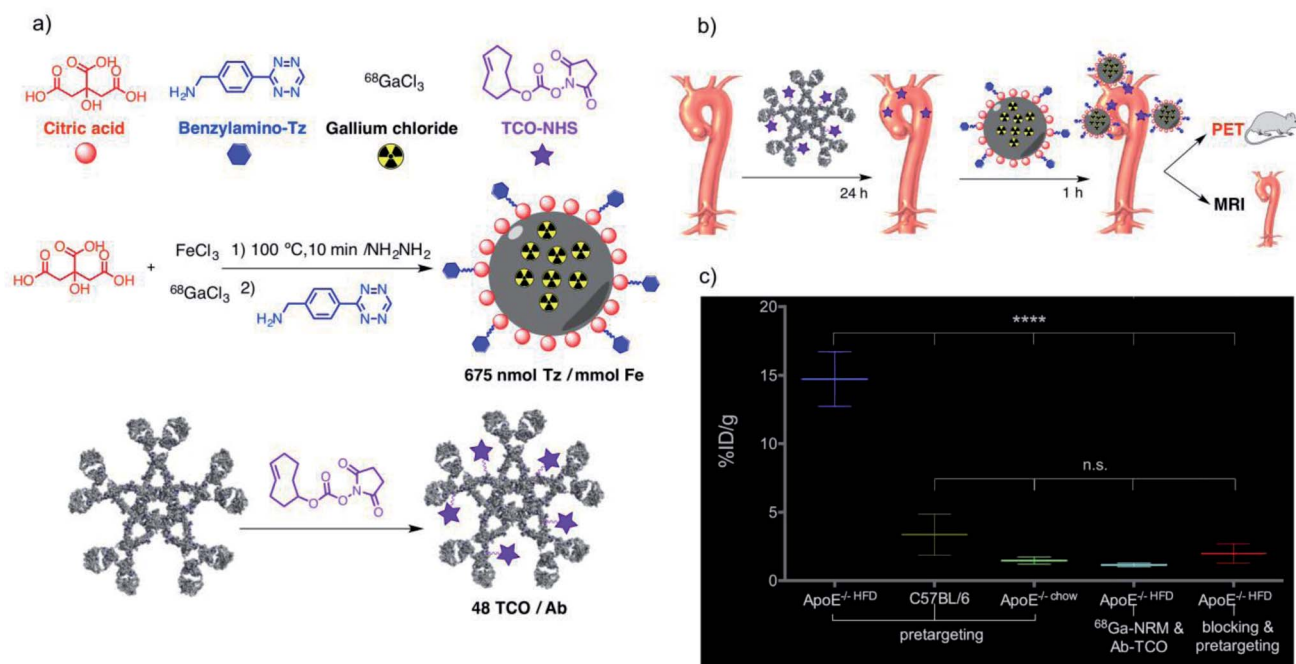
Fig. 9 (a) Preparation of ^{68}Ga core-doped iron oxide nano-radiomaterials (NRMs) with a tetrazine handle and of TCO-modified antibodies. (b) Pretargeting scheme for *in vivo* PET imaging and *ex vivo* T_1-MRI atherosclerotic lesions. (c) Radioactivity uptake in mice aortas for the five conditions tested, detected with a gamma counter 2 h post-injection and expressed as the % of injected dose per gram of tissue. Adapted from Nanomedicine - Nanotechnology, Biology, and Medicine, 17, Pellico *et al.*, "Unambiguous detection of atherosclerosis using bioorthogonal nanomaterials", 26–35, Copyright (2019), with permission from Elsevier.

importance for the *in vivo* detection of acute thrombotic events as the ones occurring in stroke.

3.4 Bioorthogonal nanoparticle amplification for improved detection and diagnostics

Despite significant advances in the development of nanoparticle-based sensing technologies, in certain instances the detection of biomolecules still remains challenging, especially when dealing with low analyte concentrations, rare targets or complex samples.[162–166] In this regard, the synergy between bioorthogonal chemistry and nanoparticles can have a tremendous potential for highly sensitive and specific detection, as we will discuss in this section. The bioorthogonal nanoparticle detection (BOND) strategy was pioneered by the group of R. Weissleder and is based on the exceptionally fast IEDDA reaction between antibodies and magneto-fluorescent nanoparticles (MFNPs), each of them suitably modified with the corresponding bioorthogonal partners (typically, *trans*-cyclooctene and tetrazine, respectively).[95] The one-step BOND strategy (BOND-1) consists in the conjugation of the antibody and the nanoparticle prior to cell incubation, while in the two-step BOND (BOND-2), cells are pretargeted with the TCO-modified antibody, which acts as a scaffold for multiple covalent attachments of Tz nanoparticles (*in situ* bioorthogonal amplification, Fig. 10).

These two versions of the BOND strategy were initially assessed by Haun *et al.* for targeting extracellular receptors on different cancer cell types, using both fluorescence and magnetic resonance techniques.[95] Three different monoclonal antibodies (modified with TCO, range of 1–30 TCO moieties/Ab) were separately used to target HER2, EpCAM and EFGR. When labelled with BOND-2, cells showed a fluorescence signal one order of magnitude higher than for labelling with BOND-1, as measured by flow cytometry. For the particular case of HER2 targeting, compared with other targeting strategies, BOND-2 presented a relative labelling efficacy 3 times higher than avidin–biotin, and 15 times higher than direct conjugation with chemical modifications such as thiol/maleimide reaction. The BOND-2 strategy was also successfully applied for the detection of the bacterial pathogen Staphylococcus aureus, using a specific combination of TCO-Ab and Tz-modified magnetic nanoprobes, which enabled detection by diagnostic magnetic resonance (DMR).[118] To further push the capability of bioorthogonal amplification and the detection sensitivity limits, Peterson *et al.* enhanced the labelling process by adding a second amplification step making use of two sets of MFNPs, each of them functionalised with Tz or TCO (*vide infra*).[97] The process, illustrated in Fig. 11a, comprises the following steps: initial cell incubation with TCO-Ab; labelling with Tz-MFNPs; amplification with TCO-MFNPs (AMP1); further amplification with Tz-MFNPs (AMP2). The click moieties were bound to the MFNPs though a disulphide bond, which allowed their cleavage after binding to their targets (noted as AMP1-C and AMP2-C) in order to perform DMR, which was found to be a much more sensitive analytical method than
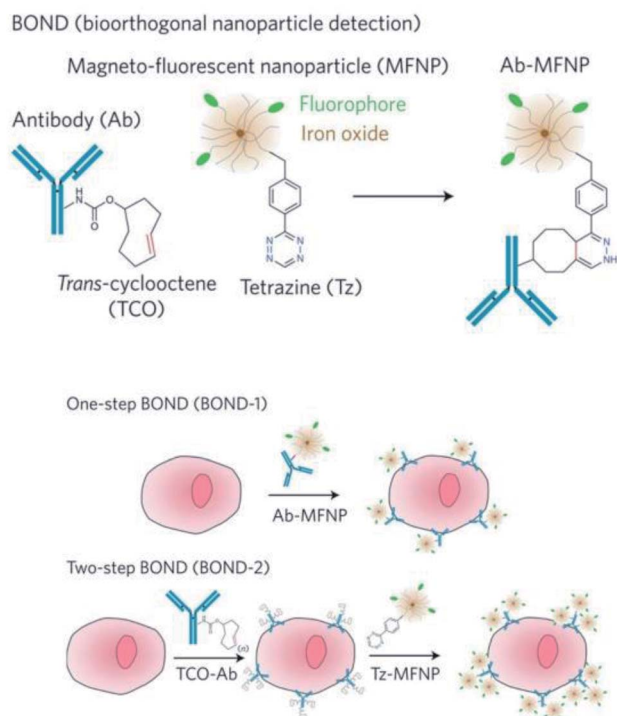
Fig. 10 Overview of the BOND strategy. Left: Covalent coupling of TCO-antibodies and Tz-MFNPs. Right: Application of the BOND strategy for one-step (direct) and two-step (bioorthogonal amplification) targeting of MFNPs to cells. Reprinted by permission from Springer Nature, Nature Nanotechnology, "Bioorthogonal chemistry amplifies nanoparticle binding and enhances the sensitivity of cell detection", J. B. Haun, N. K. Devaraj, S. A. Hilderbrand, H. Lee and R. Weissleder, Copyright (2010).

flow cytometry. SK-BR-3 human breast cancer cells were incubated with TCO-antiHER2 and then labelled with VT680-MFNP-Tz (green), FITC-MFNP-TCO (blue) and RITC-MFNP-Tz (red), confirming the success of each step, and also the proper fluorescence loss when the MFNPs were cleaved using 1,4-dithiothreitol (DTT) (Fig. 11b). When analysing the nuclear magnetic resonance (NMR) signals corresponding to the different strategies, AMP2-C showed the highest overall signal; however, AMP1-C provided the largest signal increase for consecutive steps, so it was the strategy of choice for the analysis of clinical samples, in which four pancreatic cancer biomarkers were targeted (EGFR, EpCAM, HER2 and MUC1). When using AMP1, the signal was negligible for all four biomarkers; by contrast, when cleaving the MFNPs (AMP1-C), the signals corresponding to EpCAM and especially to MUC1 were significantly enhanced (Fig. 11d).

Weissleder's group also pioneered the use of the BOND-2 strategy for the development of clinically relevant point-of-care detection tools. Using a portable micro-NMR (µNMR) device operated by a smartphone, the team established an accurate and highly sensitive diagnostic method for malignant tumours, based on the analysis of a relatively low number of cells (which translates into very low concentrations of the biomarkers of interest) from single fine-needle aspirate

biopsies.[117] Focussing on four signature biomarkers (EGFR, EpCAM, HER2 and MUC1), the bioorthogonal nanoparticle amplification/µNMR detection approach identified malignant abdominal lesions in 44 out of 50 patients (diagnosis which was further validated by standard techniques such as biopsy and imaging). This method surpassed immunochemistry, which is the gold standard in cancer diagnostics, both in terms of accuracy (96% *versus* 84% for immunochemistry) and speed (1 hour *versus* three days). Moreover, the results were validated in a second cohort of 20 patients, reaching 100% accuracy. The bioorthogonal amplification strategy was also employed for the detection of rare circulant tumour cells (CTCs) in whole blood samples from 20 ovarian cancer patients.[119] The CTCs were labelled with magnetic nanoparticles (MNPs) following the two-step BOND TCO/Tz strategy, and the magnetic signatures of the cells were then analysed using a microfluidic chip with a built-in array of eight micro-Hall magnetic detectors (µHD). By using MNPs with different sizes and magnetic responses, the approach was capable of multiplexed analysis of three different biomarkers. This strategy was strikingly superior to the conventional CellSearch approach§ for CTC detection: while CellSearch could only detect CTCs in 20% of the 20 patients, with 25% accuracy, the µHD technology identified CTCs in 100% of the samples, with 96% accuracy. Finally, BOND-2 enabled the profiling of microvesicles secreted by glioblastoma cells for real-time monitoring of the patient response to the treatment.[120] In this work, relevant protein biomarkers (CD63, EGFR and EGFRvIII) present on the surface of the microvesicles (mostly exosomes, Fig. 12a and b) were targeted first with TCO-antibodies, followed by Tz-MNPs (Fig. 12c and d); the labelled microvesicles were captured in a microfluidic chip and detected using µNMR, which turned out to be more sensitive than other detection techniques (Fig. 12e and f). The authors also showed that circulating microvesicles can be used to predict the therapeutic efficacy in glioblastoma patients, by analysing blood samples collected before and after standard therapy with radiation and temozolomide (TMZ). The calculated tumour progression index (TPI, Fig. 12g) allowed to successfully distinguish between responding and non-responding patients, while the efficacy index (η_{MV}, Fig. 12h) also revealed significant differences between the two patient groups.

3.5 Overcoming tumour heterogeneity and amplifying the tumour targeting ability of nanoplatforms in targeted cancer therapeutics

Nanoplatforms able to target a specific cell type, tissue or organ have a great potential in drug delivery. These systems are of huge interest, as they allow to tune the pharmacodynamics, kinetics, and biodistribution of the active principle. This not only can improve the performance of the drugs, but also retrieve molecules that were once discarded in the development process

§ CellSearch is the gold standard for CTC detection in the blood of patients with different types of metastatic cancers (https://www.cellsearchctc.com).
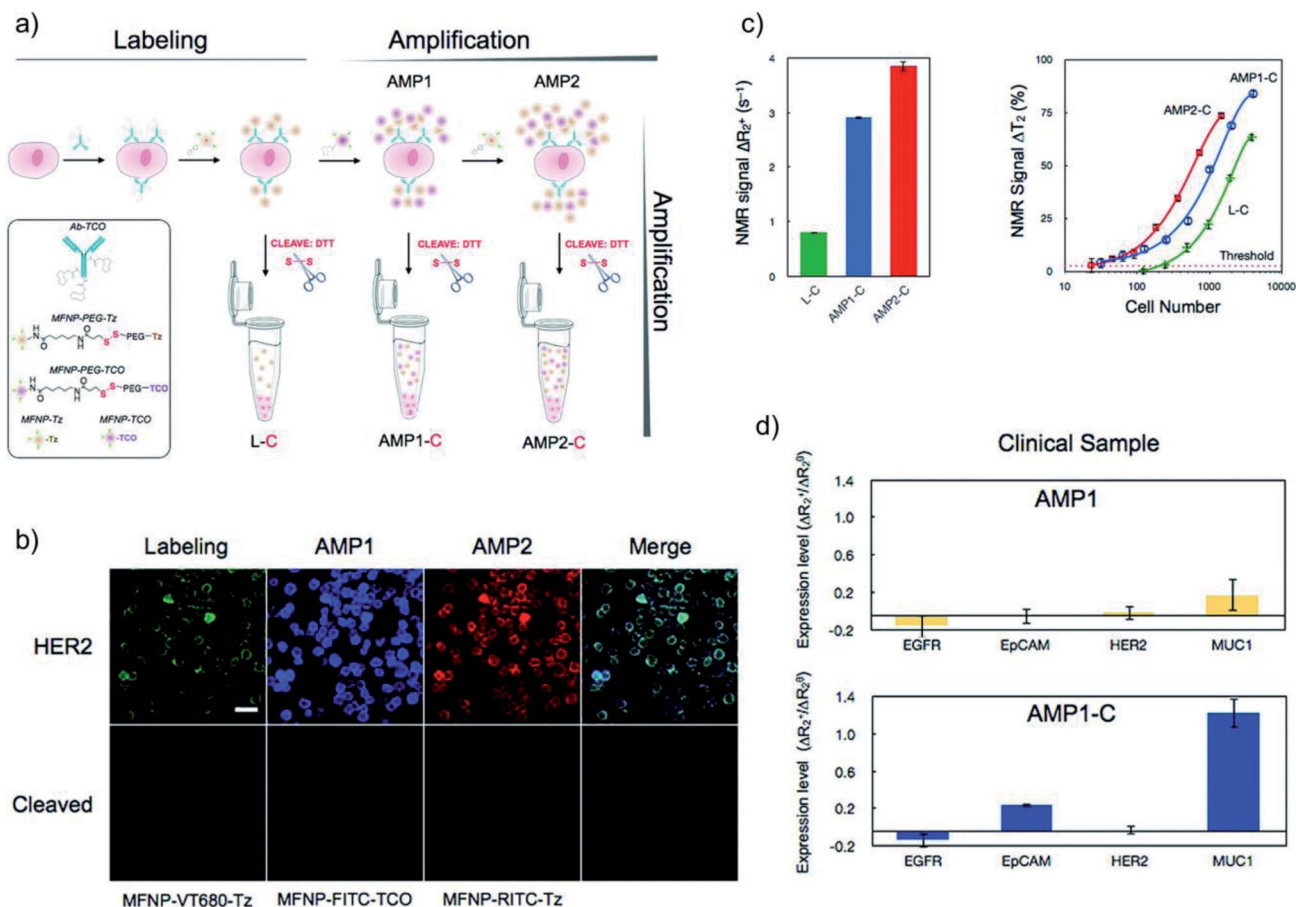
Fig. 11 (a) Scheme of the labelling, amplification and cleavage process. (b) Fluorescent images from the labelling step and subsequent amplification steps of cells presenting HER2, and cells after DTT cleavage. (c) NMR signal analysis for HER2-targeted cells and cellular detection threshold for the different cleavage methods (labelling, AMP1-C, and AMP2-C). (d) Human clinical samples from pancreatic cancer assessed with AMP1 and AMP1-C strategies for different biomarkers (EGFR, EpCAM, HER2, MUC1). Adapted with permission from ACS Nano, 6, Peterson *et al.*, "Orthogonal amplification of nanoparticles for improved diagnostic sensing", 3506–3513. Copyright (2012) American Chemical Society.

due to solubility, toxicity or stability issues, among others.[167–172] Classical nanomedicine tumour targeting approaches make use of nanoparticles modified with biological ligands (peptides, carbohydrates, antibodies, aptamers, *etc.*) that recognise receptors present on the surface of cancer cells. However, this strategy has important limitations, namely the limited availability of such receptors, the sometimes scarce difference in receptor expression between normal and tumoral cells and the heterogeneity of tumour tissues and cells in terms of types and density of receptors.[19,173] Therefore, methods able to introduce large amounts of surrogate receptors on the surface of cancer cells in a controlled, cell type-independent fashion are highly desirable. Metabolic glycoengineering offers unique opportunities in terms of generation of azide groups as artificial receptors on cell surface glycans and glycoproteins, although strategies are available also for the introduction of other types of "receptor-like" moieties, such as alkynes, tetrazines, oxyamines, *etc.* In this section of the review we discuss targeting applications based on the use of bioorthogonal chemistry and nanoparticles, highlighting the advantages of this unique combination over classical targeting approaches.

In 2012 Kim and co-workers described the first successful application of the metabolic glycoengineering approach to induce a controllable, dose-dependent expression of unnatural targets (sialic acids) on the surface of tumoral cells using Ac$_4$ManNAz as azide metabolic precursor.[105] The artificial azide receptors were targeted *via* SPAAC chemistry with PEGylated liposomes modified with a strained alkyne (DBCO-lipo); PEGylated liposomes lacking the DBCO moiety (PEG-lipo) and DBCO conjugated to a Cy5 fluorescent dye (DBCO-Cy5) were used as controls.¶ Increasing fluorescence intensity, proportional to the concentration of Ac$_4$ManNAz was observed for DBCO-lipo labelling, while PEG-lipo revealed minimal unspecific binding to the cell surface (Fig. 13a). Moreover, as it can be seen in Fig. 13b, at the same concentration of Cy5 probe, DBCO-lipo showed much higher NIRF intensity when compared to DBCO-Cy5 alone, thus indicating superior targeting ability, which was attributed to the multivalent effect of the nanoparticles. Importantly, DBCO-lipo exhibited similar targeting

---

¶ All liposomal formulations included the Cy5 dye for near-infrared fluorescence experiments *in vitro* and *in vivo*.
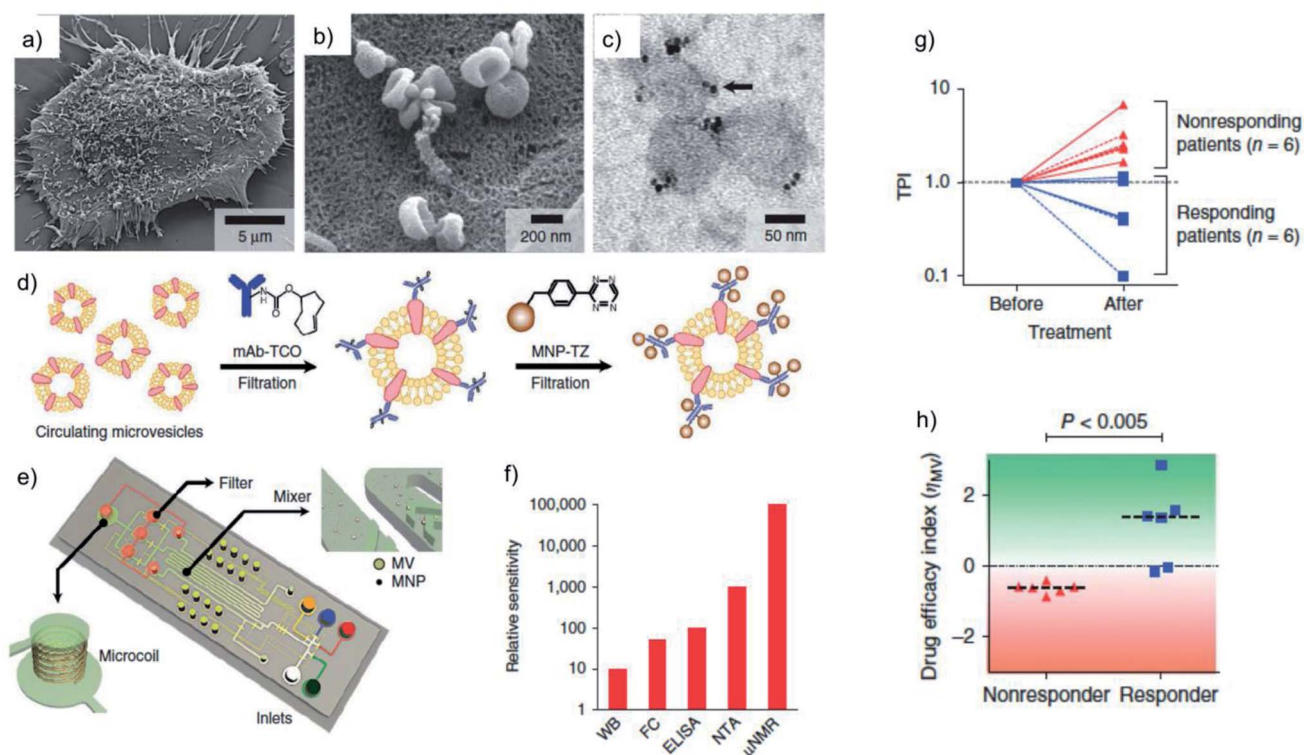
Fig. 12   μNMR analysis of glioblastoma-derived microvesicles and treatment response monitoring. (a) Scanning electron microscopy (SEM) image of a primary human glioblastoma cell, releasing abundant microvesicles. (b) High-magnification SEM image revealing saucer-shape exosomes on the surface of the cells. (c) Transmission electron microscopy (TEM) images of MNP-targeted exosomes. (d) BOND-2 strategy for the amplified binding of MNPs to protein biomarkers on the surface of microvesicles. (e) Design of the microfluidic system used for on-chip detection of circulating microvesicles. (f) Comparison of microvesicle detection sensitivity of different techniques, showing superior performance of μNMR when compared to western blotting (WB), flow cytometry (FC), enzyme-linked immunosorbent assay (ELISA) and nanoparticle tracking analysis (NTA). (g and h) Clinical trial results. Plots showing TPI values (g) and their corresponding η_{MV} values (h) from the same patients before and after combined TMZ and radiation treatment. Reprinted by permission from Springer Nature, Nature Medicine, "Protein typing of circulating microvesicles allows real-time monitoring of glioblastoma therapy", H. Shao, J. Chung, L. Balaj, A. Charest, D. D. Bigner, B. S. Carter, F. H. Hochberg, X. O. Breakefield, R. Weissleder and H. Lee, Copyright (2012).

efficiency in various types of metabolically engineered cancer cells (human lung carcinoma A549, human glioblastoma U87MG, human nasopharyngeal carcinoma KB and human breast cancer MCF7), irrespective of their heterogeneity. This dose-dependent generation of artificial azide reporters was confirmed *in vivo* in mice bearing A549 xenograft tumours and treated with increasing concentrations of Ac$_4$ManNAz administered by intra-tumoural injection in the left tumour (saline was used as control in the right flank tumours), followed by intravenous injection of DBCO-lipo, PEG-lipo and DBCO-Cy5. PEG-lipo displayed comparable NIRF intensities in both tumours (treated or not with Ac$_4$ManNAz), while DBCO-lipo showed much higher accumulation in the tumours treated with Ac$_4$ManNAz than in the saline-treated control tumours; moreover, the binding of DBCO-lipo to the pre-treated tumours was Ac$_4$ManNAz concentration-dependent (Fig. 13c). In line with the *in vitro* observations, DBCO-Cy5 gave only a faint NIRF signal and showed much lower accumulation in the tumours than DBCO-lipo, probably due to the shorter circulation time of the probe and to the lack of the multivalent effect of the

liposomes; this result suggests that the bioorthogonal chemistry-based targeting approach is more advantageous in the case of nanoparticles than in the case of small molecules.

Further work by Kim's group demonstrated that this artificial azide-reporter targeting strategy can significantly improve the tumour targeting efficiency of nanomaterials when compared to classical biological ligand methods and overcome problems related to tumour heterogeneity; the concept is illustrated in Fig. 14a. Lee *et al.*[112] developed a dendrimer-based nanosized metabolic precursor (nano-MP) with Ac$_3$ManNAz attached to the dendrimer through an ester bond that can be hydrolysed under the acidic conditions inside a tumour cell to release the free Ac$_3$ManNAz. This system surpassed the classical tumour targeting approach based on natural biological markers, showing promise for overcoming tumour heterogeneity. Incubation of different tumour cells overexpressing various receptors (cyclic RGD peptide, folate and Cetuximab) with nano-MPs yielded systematic cell membrane labelling after bioorthogonal reaction with ADIBO-Cy5.5, while treatment with the specific targeting molecule labelled with Cy5.5 only marked
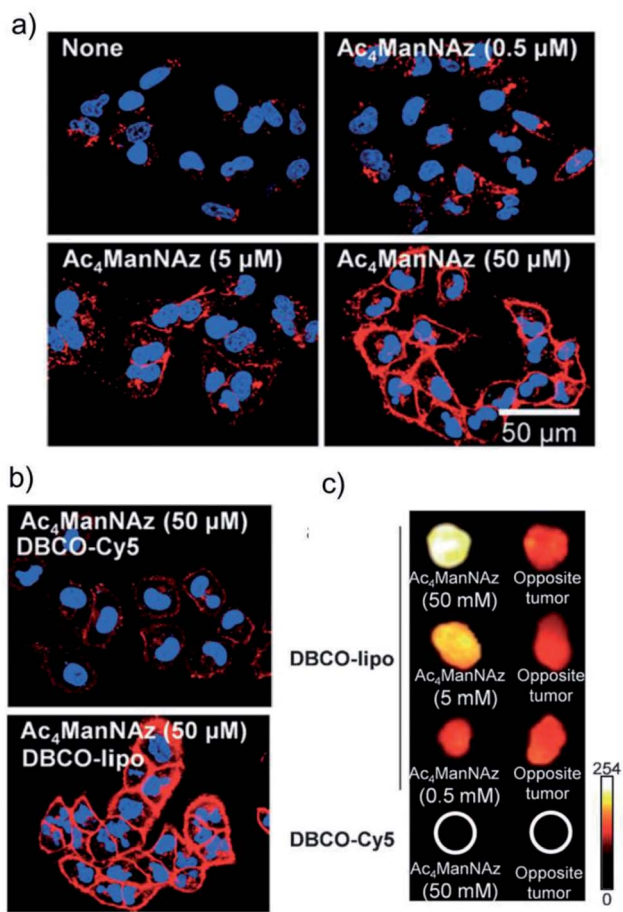
Fig. 13 (a) Dose-dependent generation of azide groups on the surface of A549 cells. (b) Fluorescence intensity enhancement due to the multivalent effect of nanoparticles at the same concentration of azide precursor. Red: DBCO. Blue: DAPI (cell nucleus stain) (c) *ex vivo* NIRF analysis of tumour tissue labelling with DBCO-lipo and DBCO-Cy5. Reprinted from Angew. Chem., Int. Ed., 51, H. Koo *et al.*, "Bioorthogonal copper-free click chemistry *in vivo* for tumor-targeted delivery of nanoparticles", 11836–11840, Copyright (2012), with permission from John Wiley & Sons Ltd.

the corresponding cell line (Fig. 14b). Yoon *et al.* compared the targeting efficiency of glycol chitosan nanoparticles (CNPs) functionalised with bicyclononyne (BCN-CNPs) or cyclic RGD (cRGD-CNPs) moieties using two cell lines labelled with azides *via* metabolic glycoengineering: U87 (showing a high level of integrin $\alpha_v\beta_3$ expression) and MCF7 (low integrin $\alpha_v\beta_3$ expression)‖.[109] *In vitro*, BCN-CNPs showed more intense and uniform fluorescence signals in both types of cells, while the cRGD-CNPs displayed strong fluorescence only in the case of U87 cells (Fig. 14c). *In vivo*, azide reporters were installed by intra-tumoural injection of Ac$_4$ManNAz in U87 tumours, followed by intravenous administration of BCN-CNPs and cRGD-CNPs; the targeting efficiency of BCN-CNPs was superior to the one of cRGD-CNPs, as demonstrated by NIRF imaging.

‖ The short peptide epitope Arg-Gly-Asp (RGD) is the common recognition motif of integrins $\alpha_v\beta_3$.

Further insights on the targeting efficiency of both CNPs in the context of tumour cell heterogeneity were obtained by incubating U87 cells isolated from the murine U87 tumours with BCN-CNPs and cRGD-CNPs. Flow cytometry analysis revealed that the percentage of cells labelled with BCN-CNPs was much higher than the one of cells decorated with cRGD-CNPs (92.9% *vs.* 50.9%). During tumour progression, U87 cells formed subpopulations with different phenotypes and levels of integrin $\alpha_v\beta_3$ expression, which led to a less effective targeting with cRGD-CNPs following the classical biological ligand approach; nevertheless, the bioorthogonal chemistry strategy was still highly effective and produced a uniform tumour cell labelling with BCN-CNPs.

Direct intra-tumoral injection of the metabolic precursor is a straightforward way of generating artificial reporters *in vivo*, but it cannot be efficiently applied to less accessible tumours. On the other hand, several studies revealed that upon intravenous administration, metabolic precursors can generate the desired reporters not only in the tumours, but also in other tissues and organs, especially in kidneys, liver and spleen, due to renal clearance and lack of tumour-targeting ability.[108,112,174] Therefore, strategies that can promote the tumour-specific generation of bioorthogonal reporters and improve the *in vivo* tumour targeting and penetration of NPs are much needed. One such strategy consists in a two-step approach based on the use of nanocontainers suitable for intravenous administration: in the first step, due to their size, the nanocontainers are able to deliver more efficiently the metabolic precursors to the tumour site on the basis of the EPR effect;[49,76,108,112] in the second step, the NPs of choice are administered also by intravenous injection, accumulate in the tumours by EPR and bind *via* bioorthogonal reactions to the "receptor-like" groups generated in the first step. Typically, the metabolic precursors were encapsulated or loaded inside glycol chitosan nanoparticles[108] or lipid nanoparticles,[76] and these systems were successfully used for targeted drug delivery and therapy in combination with a second functional NP. Lee *et al.*[108] used glycol chitosan nanoparticles (CNPs) loaded with Ac$_4$ManNAz and injected intravenously to A549 tumour-bearing mice to generate "receptor-like" azide groups on the tumour cells, which were subsequently treated with BCN-modified CNPs bearing a photosensitizer (chlorin e6, Ce6) for photodynamic therapy (BCN/Ce6-CNPs). Whole body NIRF imaging and *ex vivo* fluorescence analysis revealed a much higher tumour accumulation of BCN/Ce6-CNPs in the case of the animals treated with the CNP-azide precursors, while free Ac$_4$ManNAz injection mainly produced azide groups in the liver and kidneys, due to its lack of passive tumour targeting capability through EPR. *In vivo* photodynamic therapy using the Ac$_4$ManNAz-CNP and BCN/Ce6-CNP stepwise strategy indicated the destruction of the tumour tissue after laser irradiation (tumours reached a volume of 8.5 mm^3 three weeks post-laser treatment); conversely, in mice without Ac$_4$ManNAz–CNP pre-treatment, tumour size slowly increased in time (up to 185 mm^3), while mice treated only with free Ce6 experienced a dramatic growth of the tumours, comparable to the one of the control group (375 mm^3). Du *et al.*[76] developed a nanotheragnostic agent for
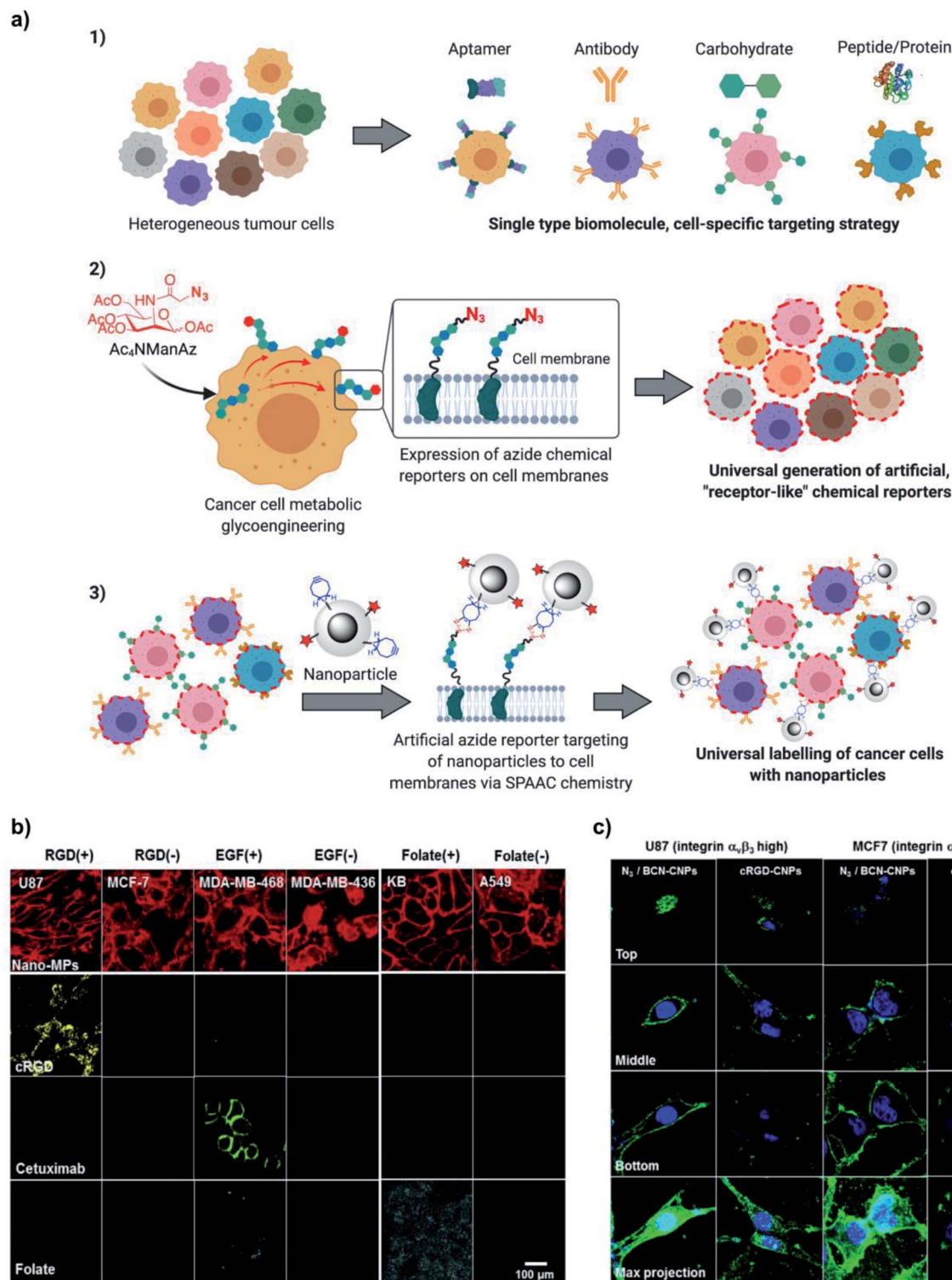
Fig. 14 (a) Universal labelling of cancer cells using the metabolic glycoengineering approach vs. specific labelling using biological receptors. Adapted with permission from Mol. Pharm., 14, H. Y. Yoon et al., "Artificial chemical reporter targeting strategy using bioorthogonal click reaction for improving active-targeting efficiency of Tumor", 1558–1570. Copyright (2017) American Chemical Society. (b) Comparative study of the tumour cell-binding ability of click molecules and biological ligands. Confocal fluorescence microscope images of tumour cells after treatment of Ac₃ManNAz-nano/ADIBO-Cy5.5 and biological ligands. ADIBO-Cy5.5 (20 mM), cRGD-Cy5.5 (10 mM), Cetuximab-Cy5.5 (10 mM), and Folate-Cy5.5 (10 mM) were visualized in red, yellow, green, and blue fluorescence (pseudo colours), respectively. Reprinted from Biomaterials, 148, S. Lee et al., "Nano-sized metabolic precursors for heterogeneous tumor-targeting strategy using bioorthogonal click chemistry in vivo", 1–15, Copyright (2017), with permission from Elsevier; (f) confocal microscopy analysis of azide reporter generation in U87 (high integrin αᵥβ₃ expression) and MCF7 (low integrin αᵥβ₃ expression) cell lines treated with FITC-labelled cRGD-CNPs or BCN-CNPs. Reprinted with permission from Mol. Pharm., 14, H. Y. Yoon et al., "Artificial chemical reporter targeting strategy using bioorthogonal click reaction for improving active-targeting efficiency of tumor", 1558–1570. Copyright (2017) American Chemical Society. Fig. 14a was created with BioRender.com.

synergistic photothermal therapy (PTT) and photoacoustic therapy (PAT) based on nanomicelles self-assembled from a lipophilic zinc(II)–phthalocyanine (ZnPc, an excellent near infrared (NIR) photoabsorbing agent for PTT and PAT) and a lipid poly(ethylene glycol) chain (LP). The metabolic azide precursor was encapsulated inside LP nanomicelles (Ac$_4$-ManNAz–LP) and delivered by intravenous injection into the tail vein of mice with subcutaneous A549 tumours, while the ZnPc–LP nanomicelles were further modified with DBCO (DBCO–ZnPc–LP) for bioorthogonal click chemistry (Fig. 15). The superior tumour targeting efficiency of the two-step strategy when compared to only the EPR effect was demonstrated by acquiring photothermal images of the tumours from three different groups of mice, treated with saline (control group), DBCO–ZnPc–LP alone and DBCO–ZnPc–LP after pre-treatment with Ac$_4$ManNAz–LP. Upon irradiation with 808 nm continuous laser, the local temperatures in the tumours of the mice subjected to the two-step strategy increased up to 45 °C in 4 min; in the same timeframe, the tumours of the group treated with DBCO–ZnPc–LP alone only reached 38 °C. To verify the synergistic effect of the photoacoustic imaging-guided dual PTT and PAT, mice with A549 tumours of 100–150 mm^3 were treated with Ac$_4$ManNAz–LP/DBCO–ZnPc–LP and subjected to the different modalities: PTT (5 min irradiation with 808 nm continuous laser at a power density of 0.1 W cm^{-2}), PAT (1 min irradiation with 808 nm pulsed laser at a power density of 0.2 W cm^{-2}) and the combination of both (the control group was treated only with saline and no therapy was applied). As it can be inferred from Fig. 14, PTT or PAT alone led to a reduction of the tumour volume only in the first days of the treatment; in contrast, the synergistic treatment showed a continuous shrinking of the tumours up to 18 days post-irradiation, without noticeable side effects.

Another stepwise strategy to enhance the penetration of drug-loaded nanoparticles into tumours consists in the pre-targeting of the cells with an antibody labelled with a click moiety, a process coined "click reaction-assisted immune cell targeting" or CRAIT.[99] Immature myeloid cells (iMCs) are typically recruited at the early stage in various tumour types to ensure protection against immune destruction and can also infiltrate deep inside the avascular regions of the tumours. In this approach, iMCs were used as a sort of Trojan horses, instead of directly targeting the cancer cells. Anti-CD11b antibodies (that will target CD11b$^+$ myeloid cells) were modified with trans-cyclooctene (TCO) and a NIR dye and administered via tail vein injection to mice bearing orthotopic 4T1 mammary carcinomas. Subsequently, tetrazine-modified mesoporous silica nanoparticles loaded with the chemotherapeutic drug doxorubicin (DOX–MSN–Tz) were also delivered by intravenous injection to react with the TCO-labelled CD11b$^+$ cells via IEDDA reaction. The modified iMCs mediated the penetration of the therapeutic NPs more deeply into the less accessible areas of the tumours and behaved as local drug reservoirs. The in vivo treatment with the CRAIT system (anti-CD11b-TCO + DOX-MSN-Tz) was found to be more efficient than all the other therapeutic options tested, inducing a 2-fold reduction of tumour growth without toxic side effects. In contrast, neither free DOX nor

DOX–MSN–Tz in the absence of the pretargeting agent anti-CD11b-TCO showed significant therapeutic effect.

Artemov and co-workers designed a two-component, two-steps strategy for the intracellular delivery of albumin (Alb)-based drug nanocarriers using antibodies modified with different click moieties (azide[91] or trans-cyclooctene[98,100]). These systems demonstrated their versatility in vitro, being used for enhanced intracellular delivery of paclitaxel (Px) in HER2-positive BT-474 breast cancer cells (pretargeting with azide-modified anti-HER2 monoclonal antibody trastuzumab (Ttz) and SPAAC reaction with Alb–Px–DBCO conjugates[91] or TCO-modified trastuzumab and IEDDA reaction with Alb–Px–Tz conjugates[98]) and mertansine (DM1) in PSMA(+) PC3-PIP prostate cancer cells (pretargeting with TCO-modified anti-PSMA 5D3 monoclonal antibody and IEDDA reaction with Alb-DM1-Tz conjugates),[100] respectively. Due to its fast kinetics, the IEDDA reaction was also evaluated in vivo in mice bearing human HER2-positive breast tumours.[98] The enhanced intracellular uptake in vitro and in vivo was associated with the formation of nanoclusters bound to the cell membrane, promoted by multiple click reactions taking place between the two components due to the overexpression of HER2 receptors on the cancer cell surface (Fig. 16a and b); these nanoclusters were rapidly internalised at 37 °C by clathrin-mediated endocytosis (Fig. 16c). In terms of therapeutic efficacy, as shown in Fig. 16d, mice pre-treated with TCO-modified trastuzumab, followed by intravenous injection of the tetrazine-albumin nanocarrier (Alb–Px–Tz), showed a significant inhibition of tumour growth in comparison with the non-treated and control animals (treated only with trastuzumab and Alb–Px–Tz). This enhanced therapeutic effect was attributed to the rapid internalisation of the nanoclusters, followed by the release of Px from the albumin nanocarrier by acidic or enzymatic cleavage inside the tumour. The main advantage of the two-component, two-steps strategy presented in this example is its high specificity: the nanocluster formation is favoured by the presence of a large number of HER2 receptors on the cell surface; therefore, the approach is not likely to work in healthy cells or cells that do not overexpress HER2 receptors.

A last two-step tumour pretargeting approach highlighted in this section makes use of pH-dependent precursors of bioorthogonal reporters. Lu et al. used a pH (low) insertion peptide (pHLIP, a soluble peptide that presents transmembrane activity in a pH-dependent manner) to incorporate tetrazine groups selectively into tumours due to the acidic tumour microenvironment.[124] These Tz groups were then targeted in vivo in mice bearing subcutaneous HeLa tumours by TCO-modified HSA nanoparticles loaded with indocyanine green (ICG) as NIR absorber for PTT (TCO-HSA-ICG, THI); THI nanoparticles accumulated in the tumour though the EPR effect and could bind to the Tz groups via IEDDA reaction. The system showed superior tumour accumulation in vivo when compared to active tumour targeting using folic acid-modified HI (FHI), which translated into an enhanced efficiency of the photothermal treatment. Tumours from pHLIP-Tz/THI-treated mice were completely ablated with no regrowth, and the animals presented a 100% survival rate after 50 days. This showed a great
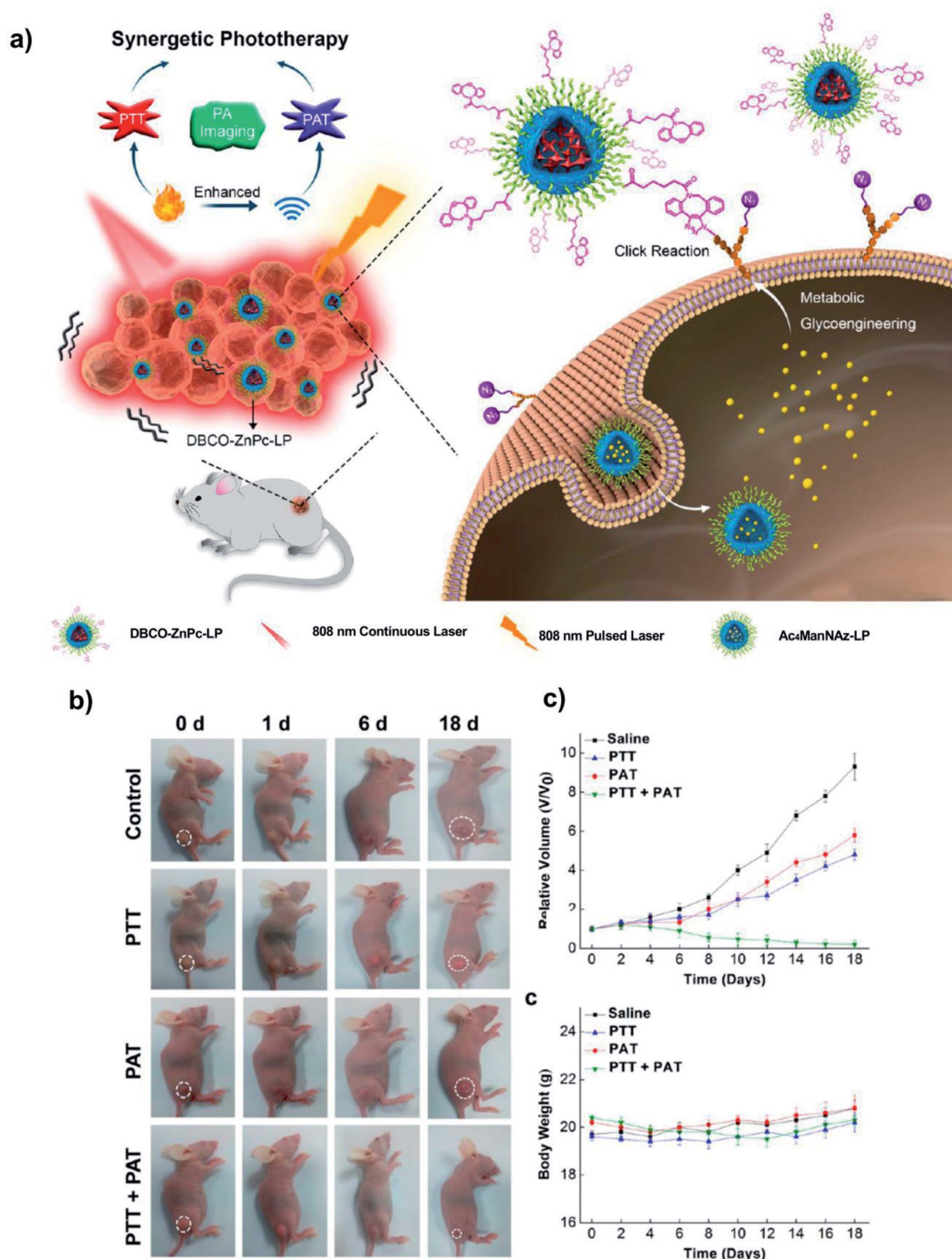
Fig. 15 (a) Schematic illustration of the photoacoustic imaging-guided synergistic PTT/PAT with the bioorthogonal metabolic glycoengineering-activated tumour targeting nanoagent. (b) Photographs of mice belonging to different groups before and after therapy. (c) Measured tumour growth (top) and body weight of mice (bottom) for 18 days after the different treatments. Reprinted with permission from ACS Nano, 11, L. Du et al., "*In vivo* imaging-guided photothermal/photoacoustic synergistic therapy with bioorthogonal metabolic glycoengineering-activated tumor targeting anoparticles", 8930–8943. Copyright (2017) American Chemical Society.
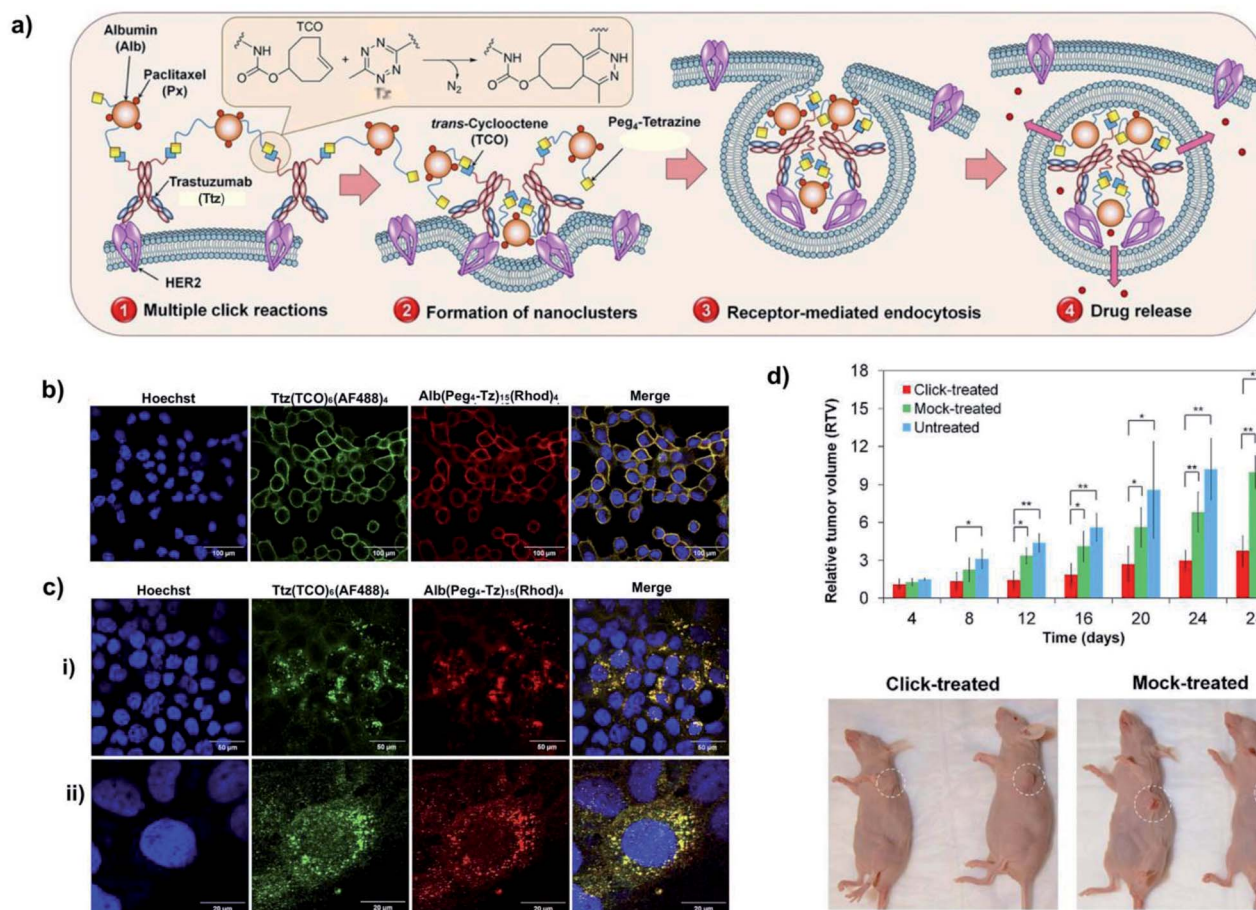
Fig. 16 (a) Illustration of the concept of biorthogonal targeted two-component, two-step drug delivery in HER2-positive cancer cells. *In vitro* confocal fluorescence images of HER2(+) BT-474 cells showing (b) cell surface labelling by trastuzumab-TCO and subsequent co-localization of albumin-tetrazine nanocarriers (green – AlexaFluor 488; red – Rhodamine; scale bar: 100 μm.) and (c) rapid cellular internalization after incubation at 37 °C (scale bar is 50 μm for the full field-of-view images in (i) and 20 μm for the zoomed-in high-resolution images in (ii). (d) Therapeutic effect of the biorthogonal targeted two-component, two-step strategy: changes in relative tumour volume (RTV = V_t/V_0) after two doses of treatment over 28 days in mice bearing BT-474 tumours and changes in tumour appearance after biorthogonal targeted therapy *versus* mock therapy. Adapted from S. Hapuarachchige, Y. Kato and D. Artemov, "Bioorthogonal two-component drug delivery in HER2(+) breast cancer mouse models", Scientific Reports, 2016, 6, 24298, Copyright 2016, Springer Nature (open access article licensed under a Creative Commons Attribution 4.0 International License).

advanced compared to the other two strategies (THI alone, without pHLIP-Tz pretargeting, and FHI) where the tumour volume increased 2 and 1.5 times, respectively, and the survival rate was 0% at day 45 for THI-treated mice and 12.5% at day 50 for FHI-treated ones.

3.6 Prodrug activation and *in situ* drug synthesis

Outside of the realm of "classical" drug delivery applications as the ones discussed in the previous sections, nanomaterials and bioorthgonal chemistry can be also used to activate prodrugs or to promote *in situ* drug synthesis from inert components. Although examples based on CuAAC, SPAAC and IEDDA are not so abundant in the literature, in this section we wish to provide a short overview of some promising recent advances (we would also like to point the interested reader in the direction of palladium-based bioorthogonal nanocatalysis that has been more extensively explored for *in situ* drug synthesis and/or

prodrug activation purposes,[32,175–182] but does not fall within the scope of this review). It is worth mentioning at this point that in several of the examples discussed in this section, bio-orthogonal bond cleavage and "click-to-release" strategies were used rather than bioorthogonal bond formation. Although less explored than the bioorthogonal ligation counterparts, bio-orthogonal bond cleavage reactions hold great potential for controlled, on-demand cargo release or activation of thera-peutic drugs and imaging probes.[183–185]

Using biocompatible entrapped copper nanoparticle catalysts (E-Cu-NPs), Clavadetscher *et al.* demonstrated the concept of *in situ* CuAAC synthesis of the anticancer drug combretastatin A4 (CA4, a tubulin polymerization inhibitor) starting from the cor-responding benign azide and alkyne precursors.[58] The cytotoxic effect of the drug was verified in HeLa and SKOV-3 cells incubated with the precursors in the presence of E-Cu-NPs; while the precursor showed no toxicity up to 10 mM concentration, the CA4
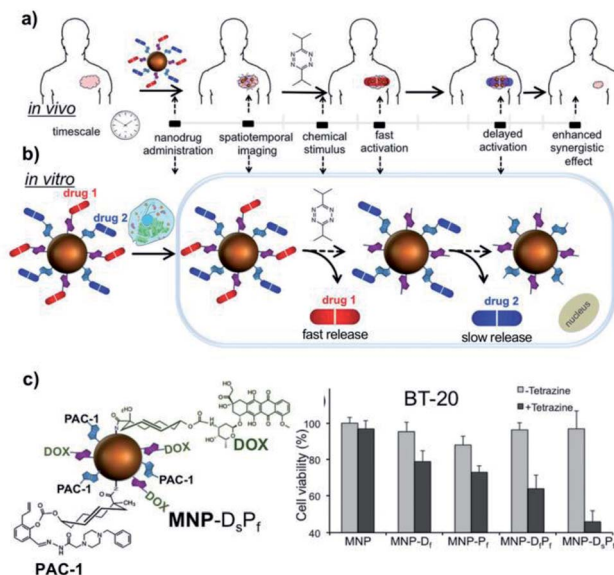
Fig. 17 a) and (b) Illustration of the concept of administration of synergistic prodrug linked to TCO and their controlled, time-staggered activation in response to a tetrazine stimulus *in vivo* and *in vitro*. (c) Therapeutic response of BT-20 TNBC cells to the controlled activation of prodrugs loaded on MNPs. Left: Schematic representation of the [PAC1−TCO$_{fast}$−MNP−TCO$_{slow}$−DOX, MNP−D$_s$P$_f$] construct, which showed the highest therapeutic efficacy. Right: Cell viability following administration of different constructs: MNP, MNP−D$_f$, MNP−P$_f$, MNP−D$_f$P$_f$ and MNP−D$_s$P$_f$ alone failed to induce cellular death, indicating inactivation of the drugs when immobilized on the MNP surface, while tetrazine administration activates the prodrugs and induces cellular death, with the greatest effect for MNP−D$_s$P$_f$ (Note: s and f stand for slow and fast, respectively). Republished with permission of The Royal Society of Chemistry, from "Single-trigger dual-responsive nanoparticles for controllable and sequential prodrug activation", N. M. Robertson, Y. Yang, I. Khan, V. E. LaMantia, M. Royzen and M. V. Yigit, Nanoscale, 2017, 9, 10020−10030; permission conveyed through Copyright Clearance Center, Inc.

triazole derivative led to a significant decrease in the cell viability, which was attributed to the arrest in the cell cycle progression. Interestingly, the nanoparticle catalyst was also functional *in vivo* in zebrafish models, as shown by the synthesis of a fluorescent triazole, indicating that the *in situ* drug synthesis could be extended to *in vivo* therapeutic applications.

A very elegant approach to controllable and sequential prodrug activation was reported by Yigit and co-workers.[122] Two synergistic chemotherapeutic drugs (doxorubicin and PAC-1) were inactivated by immobilization onto magnetic nanoparticles (chosen for their biocompatibility and their potential use as MRI contrast agents) *via* TCO and activated *in vitro* in a sequential manner using tetrazine and taking advantage of the subtle differences in the kinetics of the "click-to-release" IEEDA reaction depending on the conformation of the cyclooctene (axial substitution of TCO results in much faster release than equatorial substitution, see Fig. 17a and b). Interestingly, the synergistic effect of the therapy in nonmetastatic BT-20 triple negative breast cancer cells (BT-20 TNBC) was more accentuated when the prodrug activation was conducted sequentially than for the simultaneous activation (Fig. 17c).

Therefore, depending on the characteristics of different cancer cells, it would be possible to design tailored combination therapies in which pretreatment with a first drug could render the cells more sensitive to the effect of a second drug.

Other recent examples also clearly highlight the potential of the "click-to-release" approach for therapeutic applications in combination with nanoparticles. Wu and co-workers described a theragnostic system based on the uncaging of a vinyl ether-camptothecin prodrug (encapsulated inside liposomal nanoformulations to promote is accumulation in tumours by EPR effect) by tetrazine-modified gold nanorods (acting both as heat mediators for photothermal therapy and as contrast agents for multispectral optoacoustic tomography, MSOT), with the subsequent *in vitro* and *in vivo* activation of the drug.[130] Using a less conventional bioorthogonal reaction (strain-promoted iminosydnone–cycloalkyne cycloaddition, SPICC), Porte *et al.* developed cleavable micelles that can suffer a precisely controlled enzymatic disassembly only inside solid tumours.[137] Although the proof-of-concept was demonstrated *in vitro* and *in vivo* only for the controlled release of a fluorophore, the system is expected to be extended to other biologically relevant molecules. In a similar approach, Zuo *et al.* designed tumour microenvironment-responsive micellar nanoparticles camouflaging pro-doxorubicin (TCO-Dox) and a tetrazine partner, [4-(6-methyl-1,2,4,5-tetrazin-3-yl)phenyl]methanamine.[133] The nanovehicles, responding to specific features of the tumour microenvironment, namely low pH and tumour matrix metalloproteinase 2 (MMP2), were administered systemically to 4T1 breast tumour-bearing mice and passively accumulated in tumours by virtue of the EPR effect. Their simultaneous dissociation inside the tumours resulted in the release of the cargos and the subsequent prodrug activation through the IEDDA reaction. Importantly, although the nanovehicles also accumulated in the livers of the animals, the content of free doxorubicin was much lower in this organ than in the tumours, confirming the precise and controlled activation of the prodrug in the tumours, with a considerable decrease of the adverse effects typically associated with chemotherapy.

4. Conclusion and perspectives

In recent years, bioorthogonal chemistries in tandem with nanoparticles have demonstrated tremendous potential for the field of biomedical applications. As we have discussed at length in this review, by making the most of the unique features and capabilities of nanoparticles and the robustness and efficacy of bioorthogonal reactions, it is possible to develop more sensitive bioimaging and detection tools, as well as more efficient therapeutic systems. Due to their multivalency, nanoparticles can act as signal amplifiers, leading to more sensitive imaging probes and can induce a more efficient receptor binding for targeting applications. The introduction of artificial "receptor-like" groups onto cell surfaces in a controlled, dose-dependent fashion by metabolic engineering makes possible universal targeting strategies that do not rely on the presence of biological receptors. This not only can improve our current targeting strategies that are mostly based on receptor–ligand recognition

(or, in the case of cancer nanotherapy, on passive targeting based on the EPR effect), but also help tackling tumour heterogeneity, which is currently a major obstacle for many oncological therapies.

Despite all these advances, we believe that further developments and improvements will continue to take place in different areas. For example, the examples discussed here rely on single bioorthogonal reactions. The use of sequential, mutually orthogonal bioorthogonal chemistries and of dual-bioorthogonally-reactive handles could open up new avenues for multiplexed imaging and detection.[186,187] Workentin's group recently showed that it is possible to use up to four different bioorthogonal reactions in an interchangeable manner for attaching, replacing and releasing molecules from a nanoparticle system.[188] Nevertheless, this task is far from trivial, as the approach requires a very careful design of reagents and reactions that meet simultaneously the stringent criteria for bioorthogonality and are compatible with colloidal nanoparticles. This bring us to another area in which we envisage important advances on the short term, namely the development of new (or more robust) bioorthogonal reagents for nanoparticle functionalisation. Such new reagents should ideally have very fast kinetics, high stability, and be hydrophilic enough so that they do not pose a threat to the colloidal stability of the nanoparticles. Future breakthroughs regarding biomedical applications could also arise from the use of bioorthogonal chemistry to uncage active biomolecules and drugs *in vitro* and *in vivo* with high spatiotemporal control through the so-called "click to release" strategy. Promising steps in this direction were already taken, as described in Section 3.6, although bioorthogonal uncaging reactions remain less explored than the corresponding bond-formation ones.

Finally, future efforts should be devoted to translational aspects of the different technologies developed. As highlighted in Section 3.4, there are already some successful examples of clinical applications of IEDDA bioorthogonal chemistry in combination with magnetic nanoparticles, and we hope to see more exciting developments in this direction in the coming years, involving other types of nanoparticles and bioorthogonal reactions.

Conflicts of interest

There are no conflicts to declare.

List of abbreviations

4T1	Mouse breast cancer cell line
A549	Human lung adenocarcinoma cell line
Ab	Antibody
Ac$_{3/4}$ManNAz	*N*-Azidoacetylmannosamine, tri/tetraacetylated
Ad	Adamantane
ADIBO	Azadibenzocyclooctyne‡
Alb	Albumin
ApoE	Apolipoprotein E
AuNP	Gold nanoparticle
BARAC	Biarylazacyclooctynone
BCN	Bicyclo[6.1.0]non-4-yne
BCN-dual-NP	BCN-conjugated glycol chitosan nanoparticle
BONCAT	Bioorthogonal noncanonical amino acid tagging
BOND	Bioorthogonal nanoparticle detection
BT-20 TNBC	BT-20 triple negative breast cancer cells
BT-474	Human breast cancer cell line
CA4	Combretastatin A4
CD	Cyclodextrin
CD41	Integrin alpha chain 2b
Ce6	Chlorin e6
CHO	Chinese hamster ovary cell line
CNP	Chitosan nanoparticle
CQDot	Carbon quantum dot
CRAIT	Click reaction-assisted immune cell targeting
CT	Computed tomography
CTC	Circulant tumour cell
CuAAC	Copper-catalysed azide–alkyne [3+2] cycloaddition
CXCR4	C–X–C chemokine receptor type 4
Cy	Cyanine
DBCO	Dibenzocyclooctyne
DM1	Mertansine
DMR	Diagnostic magnetic resonance
DNBA	5,5′-dithiobis(2-nitrobenzoic acid)
DTT	1,4-Dithiothreitol
EGFR	Epidermal growth factor receptor
ELISA	Enzyme-linked immunosorbent assay
EpCAM	Epithelial cell adhesion molecule, CD326
EPR	Enhanced permeation and retention effect
FA	Folic acid
FC	Flow cytometry
FITC	Fluorescein isothiocyanate
FND	Fluorescent nanodiamond
FR	Folate receptor
GalNAz	*N*-Azidoacetylgalactosamine
GlcNAz	*N*-Azidoacetylglucosamine
HAuNP	Hollow gold nanoparticle
HCA	Hemicyanine
HD	Hall magnetic detector
HeLa	Human cervical carcinoma cell line
HEp-2	Human epidermal larynx carcinoma cell line
HER2	Human epidermal growth factor receptor 2
HFW	Human fibroblasts cell line
hMSC	Human mesenchymal stem cell
HPGFND	Hyperbranched-polyglycerol-coated fluorescent nanodiamond
ID	Injected dose
IEDDA	Inverse electron-demand Diels–Alder
iMC	Immature myeloid cell
IONP	Iron oxide nanoparticle

‡ In the literature, ADIBO and DBCO are both used to refer to the same structure (see Fig. 2b).

KB	Human nasopharyngeal epidermoid carcinoma cell line
LP	Lipid poly(ethylene glycol) chain
ManNAz	N-Azidoacetylmannosamine
MCF7	Human breast adenocarcinoma cell line
MFNP	Magneto-fluorescent nanoparticle
MMP2/9	Tumour matrix metalloproteinases 2 and 9
MNP	Magnetic nanoparticle
MR	Magnetic resonance
MRI	Magnetic resonance imaging
MSOT	Multispectral optoacoustic tomography
MSN	Mesoporous silica nanoparticle
MUC1	Mucin 1, cell surface associated
Nano-MP	Nanosized metabolic precursor
NB	Norbornene
NIR	Near infrared
NIRF	Near infrared fluorescence
NLS	Nuclear localization sequence
NMR	Nuclear magnetic resonance
NP	Nanoparticle
NRM	Nano-radiomaterial
NTA	Nanoparticle tracking analysis
PDots	Polymer dots
oxLDL	Oxidised low-density lipoprotein
PAMAM	Polyamidoamine
PAT	Photoacoustic therapy
Pc	Phthalocyanine
PC3-PIP	Human prostate cancer cell line
PDot	Polymer dot
PEG	Polyethylene glycol
PEI	Polyethylenimine
PET	Positron emission tomography
PFBT	Poly[(9,9-dioctylfluorenyl-2,7-diyl)-co-(1,4-benzo-{2,1′,3}-thiadiazole)]
pHLIP	pH (low) insertion peptide
PSMA	Poly(styrene-co-maleic anhydride) and prostate specific membrane antigen, see context
PTS	Photothrombotic stroke
PTT	Photothermal therapy
Px	Paclitaxel
QDot	Quantum dot
RITC	Rhodamine B isothiocyanate
RGD	Arginylglycylaspartic acid
RTV	Relative tumour volume
SEM	Scanning electron microscopy
SERS	Surface-enhanced Raman spectroscopy
SiaNAz	N-Azidoacetylsialic acid
SK-BR-3	Human breast cancer cell line
SKOV-3	Human ovarian cancer cell line
SNP	Supramolecular nanoparticle
SPAAC	Strain-promoted azide–alkyne [3+2] cycloaddition
SPICC	Strain-promoted iminosydnone-cycloalkyne cycloaddition
SWCNTs	Single-walled carbon nanotubes
TCO	Trans-cyclooctene
TEM	Transmission electron microscopy
TMZ	Temozolomide
TPI	Tumour progression index
Ttz	Trastuzumab

Tz	Tetrazine
U87	Human glioblastoma cell line
US	Ultrasound
VT680	VivoTag-S 680 fluorochrome
WB	Western blotting

Acknowledgements

References

1 T. L. Doane and C. Burda, The unique role of nanoparticles in nanomedicine: imaging, drug delivery and therapy, Chem. Soc. Rev., 2012, 41, 2885.

2 J. Mosayebi, M. Kiyasatfar and S. Laurent, Synthesis, Functionalization, and Design of Magnetic Nanoparticles for Theranostic Applications, Adv. Healthcare Mater., 2017, 6, 1700306.

3 N. R. Datta, S. Krishnan, D. E. Speiser, E. Neufeld, N. Kuster, S. Bodis and H. Hofmann, Magnetic nanoparticle-induced hyperthermia with appropriate payloads: Paul Ehrlich's "magic (nano)bullet" for cancer theranostics?, Cancer Treat. Rev., 2016, 50, 217–227.

4 D.-E. Lee, H. Koo, I.-C. Sun, J. H. Ryu, K. Kim and I. C. Kwon, Multifunctional nanoparticles for multimodal imaging and theragnosis, Chem. Soc. Rev., 2012, 41, 2656–2672.

5 N. Bertrand, J. Wu, X. Xu, N. Kamaly and O. C. Farokhzad, Cancer nanotechnology: The impact of passive and active targeting in the era of modern cancer biology, Adv. Drug Delivery Rev., 2014, 66, 2–25.

6 R. M. Fratila, S. G. Mitchell, P. Del Pino, V. Grazu and J. M. De La Fuente, Strategies for the biofunctionalization of gold and iron oxide nanoparticles, Langmuir, 2014, 30, 15057–15071.

7 H. Maeda, Toward a full understanding of the EPR effect in primary and metastatic tumors as well as issues related to its heterogeneity, *Adv. Drug Delivery Rev.*, 2015, **91**, 3–6.

8 *Handbook of Nanomaterials for Cancer Theranostics*, ed. J. Conde, Elsevier, 1st edn, 2018.

9 A. M. Dennis, J. B. Delehanty and I. L. Medintz, Emerging Physicochemical Phenomena along with New Opportunities at the Biomolecular–Nanoparticle Interface, *J. Phys. Chem. Lett.*, 2016, **7**, 2139–2150.

10 D. A. Scheinberg, J. Grimm, D. A. Heller, E. P. Stater, M. Bradbury and M. R. McDevitt, Advances in the clinical translation of nanotechnology, *Curr. Opin. Biotechnol.*, 2017, **46**, 66–73.

11 A. Arsiwala, A. Castro, S. Frey, M. Stathos and R. S. Kane, Designing Multivalent Ligands to Control Biological Interactions: From Vaccines and Cellular Effectors to Targeted Drug Delivery, *Chem.–Asian J.*, 2019, **14**, 244–255.

12 J. A. Prescher and C. R. Bertozzi, Chemistry in living systems, *Nat. Chem. Biol.*, 2005, **1**, 13–21.

13 E. M. Sletten and C. R. Bertozzi, Bioorthogonal chemistry: Fishing for selectivity in a sea of functionality, *Angew. Chem., Int. Ed.*, 2009, **48**, 6974–6998.

14 E. M. Sletten and C. R. Bertozzi, From Mechanism to Mouse: A Tale of Two Bioorthogonal Reactions, *Acc. Chem. Res.*, 2011, **44**, 666–676.

15 A. Borrmann and J. C. M. van Hest, Bioorthogonal chemistry in living organisms, *Chem. Sci.*, 2014, **5**, 2123.

16 H. C. Kolb, M. G. Finn and K. B. Sharpless, Click chemistry: Diverse chemical function from a few good reactions, *Angew. Chem., Int. Ed.*, 2001, **40**, 2004–2021.

17 R. K. V Lim and Q. Lin, Photoinducible bioorthogonal chemistry: A spatiotemporally controllable tool to visualize and perturb proteins in live cells, *Acc. Chem. Res.*, 2011, **44**, 828–830.

18 N. K. Devaraj and R. Weissleder, Biomedical Applications of Tetrazine Cycloadditions, *Acc. Chem. Res.*, 2011, **44**, 816–827.

19 H. Y. Yoon, H. Koo, K. Kim and I. C. Kwon, Molecular imaging based on metabolic glycoengineering and bioorthogonal click chemistry, *Biomaterials*, 2017, **132**, 28–36.

20 T. S. Lee, Y. Kim, W. Zhang, I. H. Song and C. H. Tung, Facile metabolic glycan labeling strategy for exosome tracking, *Biochim. Biophys. Acta, Gen. Subj.*, 2018, **1862**, 1091–1100.

21 S. Song, M. K. Shim, S. Lim, Y. Moon, S. Yang, J. Kim, Y. Hong, H. Y. Yoon, I.-S. Kim, K. Y. Hwang and K. Kim, In Situ One-Step Fluorescence Labeling Strategy of Exosomes *via* Bioorthogonal Click Chemistry for Real-Time Exosome Tracking In Vitro and In Vivo, *Bioconjugate Chem.*, 2020, **31**, 1562–1574.

22 H. I. Yoon, J. Y. Yhee, J. H. Na, S. Lee, H. Lee, S. W. Kang, H. Chang, J. H. Ryu, S. Lee, I. C. Kwon, Y. W. Cho and K. Kim, Bioorthogonal Copper Free Click Chemistry for Labeling and Tracking of Chondrocytes In Vivo, *Bioconjugate Chem.*, 2016, **27**, 927–936.

23 S. Lee, H. I. Yoon, J. H. Na, S. Jeon, S. Lim, H. Koo, S. S. Han, S. W. Kang, S. J. Park, S. H. Moon, J. H. Park, Y. W. Cho, B. S. Kim, S. K. Kim, T. Lee, D. Kim, S. Lee, M. G. Pomper, I. C. Kwon and K. Kim, In vivo stem cell tracking with imageable nanoparticles that bind bioorthogonal chemical receptors on the stem cell surface, *Biomaterials*, 2017, **139**, 12–29.

24 J. P. Meyer, P. Adumeau, J. S. Lewis and B. M. Zeglis, Click Chemistry and Radiochemistry: The First 10 Years, *Bioconjugate Chem.*, 2016, **27**, 2791–2807.

25 B. L. Oliveira, Z. Guo and G. J. L. Bernardes, Inverse electron demand Diels–Alder reactions in chemical biology, *Chem. Soc. Rev.*, 2017, **46**, 4895–4950.

26 M. Yang, J. Li and P. R. Chen, Transition metal-mediated bioorthogonal protein chemistry in living cells, *Chem. Soc. Rev.*, 2014, **43**, 6511–6526.

27 H. Koo, M. Choi, E. Kim, S. K. Hahn, R. Weissleder and S. H. Yun, Bioorthogonal Click Chemistry-Based Synthetic Cell Glue, *Small*, 2015, **11**, 6458–6466.

28 Y. Yuan, D. Li, J. Zhang, X. Chen, C. Zhang, Z. Ding, L. Wang, X. Zhang, J. Yuan, Y. Li, Y. Kang and G. Liang, Bridging cells of three colors with two bio-orthogonal click reactions, *Chem. Sci.*, 2015, **6**, 6425–6431.

29 M. K. Rahim, R. Kota, S. Lee and J. B. Haun, Bioorthogonal chemistries for nanomaterial conjugation and targeting, *Nanotechnol. Rev.*, 2013, **2**, 215–227.

30 K. Seidi, H. A. Neubauer, R. Moriggl, R. Jahanban-Esfahlan and T. Javaheri, Tumor target amplification: Implications for nano drug delivery systems, *J. Controlled Release*, 2018, **275**, 142–161.

31 B. Rubio-Ruiz, J. T. Weiss and A. Unciti-Broceta, Efficient Palladium-Triggered Release of Vorinostat from a Bioorthogonal Precursor, *J. Med. Chem.*, 2016, **59**, 9974–9980.

32 M. Sancho-Albero, B. Rubio-Ruiz, A. M. Pérez-López, V. Sebastián, P. Martín-Duque, M. Arruebo, J. Santamaría and A. Unciti-Broceta, Cancer-derived exosomes loaded with ultrathin palladium nanosheets for targeted bioorthogonal catalysis, *Nat. Catal.*, 2019, **2**, 864–872.

33 Y. Chen, Y. Xianyu, J. Wu, B. Yin and X. Jiang, Click chemistry-mediated nanosensors for biochemical assays, *Theranostics*, 2016, **6**, 969–985.

34 M. Colombo, S. Sommaruga, S. Mazzucchelli, L. Polito, P. Verderio, P. Galeffi, F. Corsi, P. Tortora and D. Prosperi, Site-Specific Conjugation of ScFvs Antibodies to Nanoparticles by Bioorthogonal Strain-Promoted Alkyne-Nitrone Cycloaddition, *Angew. Chem., Int. Ed.*, 2012, **51**, 496–499.

35 E. Lallana, E. Fernandez-Megia and R. Riguera, Surpassing the Use of Copper in the Click Functionalization of Polymeric Nanostructures: A Strain-Promoted Approach, *J. Am. Chem. Soc.*, 2009, **131**, 5748–5750.

36 W. R. Algar, D. E. Prasuhn, M. H. Stewart, T. L. Jennings, J. B. Blanco-Canosa, P. E. Dawson and I. L. Medintz, The controlled display of biomolecules on nanoparticles: a challenge suited to bioorthogonal chemistry, *Bioconjugate Chem.*, 2011, **22**, 825–858.

37 R. Aufaure, J. Hardouin, N. Millot, L. Motte, Y. Lalatonne and E. Guénin, Tetrazine Click Chemistry for the Modification of 1-Hydroxy-1,1-methylenebisphosphonic Acids: Towards Bio-orthogonal Functionalization of Gold Nanoparticles, *Chem.–Eur. J.*, 2016, **22**, 16022–16027.

38 W. Luo, P. Gobbo, C. D. McNitt, D. A. Sutton, V. V. Popik and M. S. Workentin, "Shine & Click" Photo-Induced Interfacial Unmasking of Strained Alkynes on Small Water-Soluble Gold Nanoparticles, *Chem.–Eur. J.*, 2017, **23**, 1052–1059.

39 R. M. Fratila, M. Navascuez, J. Idiago-López, M. Eceiza, J. I. Miranda, J. M. Aizpurua and J. M. de la Fuente, Covalent immobilisation of magnetic nanoparticles on surfaces *via* strain-promoted azide–alkyne click chemistry, *New J. Chem.*, 2017, 10835–10840.

40 C. M. Madl and S. C. Heilshorn, Bioorthogonal Strategies for Engineering Extracellular Matrices, *Adv. Funct. Mater.*, 2018, **28**, 1–21.

41 Y. Jiang, J. Chen, C. Deng, E. J. Suuronen and Z. Zhong, Click hydrogels, microgels and nanogels: Emerging platforms for drug delivery and tissue engineering, *Biomaterials*, 2014, **35**, 4969–4985.

42 E. Lallana, A. Sousa-Herves, F. Fernandez-Trillo, R. Riguera and E. Fernandez-Megia, Click Chemistry for Drug Delivery Nanosystems, *Pharm. Res.*, 2012, **29**, 1–34.

43 H. He and C. Gao, Click Chemistry on Nano-Surfaces, *Curr. Org. Chem.*, 2011, **15**, 3667–3691.

44 E. Saxon and C. R. Bertozzi, Cell Surface Engineering by a Modified Staudinger Reaction, *Science*, 2000, **287**, 2007–2010.

45 C. I. Schilling, N. Jung, M. Biskup, U. Schepers and S. Bräse, Bioconjugation *via* azide-Staudinger ligation: an overview, *Chem. Soc. Rev.*, 2011, **40**, 4840–4871.

46 Z.-P. A. Wang, C.-L. Tian and J.-S. Zheng, The recent developments and applications of the traceless-Staudinger reaction in chemical biology study, *RSC Adv.*, 2015, **5**, 107192–107199.

47 P. Gobbo, W. Luo, S. J. Cho, X. Wang, M. C. Biesinger, R. H. E. Hudson and M. S. Workentin, Small gold nanoparticles for interfacial Staudinger-Bertozzi ligation, *Org. Biomol. Chem.*, 2015, **13**, 4605–4612.

48 W. Luo, P. Gobbo, P. N. Gunawardene and M. S. Workentin, Fluorogenic Gold Nanoparticle (AuNP) Substrate: A Model for the Controlled Release of Molecules from AuNP Nanocarriers *via* Interfacial Staudinger-Bertozzi Ligation, *Langmuir*, 2017, **33**, 1908–1913.

49 P. Zhang, X. Zhang, C. Li, S. Zhou, W. Wu and X. Jiang, Target-Amplified Drug Delivery of Polymer Micelles Bearing Staudinger Ligation, *ACS Appl. Mater. Interfaces*, 2019, **11**, 32697–32705.

50 V. V. Rostovtsev, L. G. Green, V. V. Fokin and K. B. Sharpless, A Stepwise Huisgen Cycloaddition Process: Copper(I)-Catalyzed Regioselective "Ligation" of Azides and Terminal Alkynes, *Angew. Chem., Int. Ed.*, 2002, **41**, 2596–2599.

51 C. W. Tornøe, C. Christensen and M. Meldal, Peptidotriazoles on solid phase: [1,2,3]-Triazoles by regiospecific copper(I)-catalyzed 1,3-dipolar cycloadditions of terminal alkynes to azides, *J. Org. Chem.*, 2002, **67**, 3057–3064.

52 M. F. Debets, J. C. M. van Hest and F. P. J. T. Rutjes, Bioorthogonal labelling of biomolecules: new functional handles and ligation methods, *Org. Biomol. Chem.*, 2013, **11**, 6439–6455.

53 D. M. Patterson, L. A. Nazarova and J. A. Prescher, Finding the right (bioorthogonal) chemistry, *ACS Chem. Biol.*, 2014, **9**, 592–605.

54 N. Li and W. H. Binder, Click-chemistry for nanoparticle-modification, *J. Mater. Chem.*, 2011, **21**, 16717.

55 H.-S. Han, N. K. Devaraj, J. Lee, S. A. Hilderbrand, R. Weissleder and M. G. Bawendi, Development of a Bioorthogonal and Highly Efficient Conjugation Method for Quantum Dots Using Tetrazine–Norbornene Cycloaddition, *J. Am. Chem. Soc.*, 2010, **132**, 7838–7839.

56 D. C. Kennedy, C. S. McKay, M. C. B. Legault, D. C. Danielson, J. A. Blake, A. F. Pegoraro, A. Stolow, Z. Mester and J. P. Pezacki, Cellular consequences of copper complexes used to catalyze bioorthogonal click reactions, *J. Am. Chem. Soc.*, 2011, **133**, 17993–18001.

57 C. S. McKay and M. G. Finn, Click chemistry in complex mixtures: Bioorthogonal bioconjugation, *Chem. Biol.*, 2014, **21**, 1075–1101.

58 J. Clavadetscher, S. Hoffmann, A. Lilienkampf, L. Mackay, R. M. Yusop, S. A. Rider, J. J. Mullins and M. Bradley, Copper Catalysis in Living Systems and In Situ Drug Synthesis, *Angew. Chem., Int. Ed.*, 2016, **55**, 15662–15666.

59 V. Hong, N. F. Steinmetz, M. Manchester and M. G. Finn, Labeling Live Cells by Copper-Catalyzed Alkyne–Azide Click Chemistry, *Bioconjugate Chem.*, 2010, **21**, 1912–1916.

60 D. Soriano Del Amo, W. Wang, H. Jiang, C. Besanceney, A. Yan, M. Levy, Y. Liu, F. L. Marlow and P. Wu, Biocompatible copper (I) catalysts for in vivo imaging of glycans, *J. Am. Chem. Soc.*, 2010, **132**, 16893–16899.

61 C. Besanceney-Webler, H. Jiang, T. Zheng, L. Feng, D. Soriano Del Amo, W. Wang, L. M. Klivansky, F. L. Marlow, Y. Liu and P. Wu, Increasing the efficacy of bioorthogonal click reactions for bioconjugation: A comparative study, *Angew. Chemie., Int. Ed.*, 2011, **50**, 8051–8056.

62 Y. Bai, X. Feng, H. Xing, Y. Xu, B. K. Kim, N. Baig, T. Zhou, A. A. Gewirth, Y. Lu, E. Oldfield and S. C. Zimmerman, A Highly Efficient Single-Chain Metal–Organic Nanoparticle Catalyst for Alkyne–Azide "Click" Reactions in Water and in Cells, *J. Am. Chem. Soc.*, 2016, **138**, 11077–11080.

63 N. J. Agard, J. A. Prescher and C. R. Bertozzi, A strain-promoted [3 + 2] azide-alkyne cycloaddition for covalent modification of biomolecules in living systems, *J. Am. Chem. Soc.*, 2004, **126**, 15046–15047.

64 J. C. Jewett and C. R. Bertozzi, Cu-free click cycloaddition reactions in chemical biology, *Chem. Soc. Rev.*, 2010, **39**, 1272–1279.

65 J. Dommerholt, F. P. J. T. Rutjes and F. L. van Delft, Strain-Promoted 1,3-Dipolar Cycloaddition of Cycloalkynes and Organic Azides, *Top. Curr. Chem.*, 2016, **374**, 16.

66 C. J. Pickens, S. N. Johnson, M. M. Pressnall, M. A. Leon and C. J. Berkland, Practical Considerations, Challenges, and Limitations of Bioconjugation *via* Azide–Alkyne Cycloaddition, *Bioconjugate Chem.*, 2018, **29**, 686–701.

67 J. C. Jewett, E. M. Sletten and C. R. Bertozzi, Rapid Cu-Free Click Chemistry with Readily Synthesized Biarylazacyclooctynones, *J. Am. Chem. Soc.*, 2010, **132**, 3688–3690.

68 N. J. Agard, J. M. Baskin, J. A. Prescher, A. Lo and C. R. Bertozzi, A Comparative Study of Bioorthogonal Reactions with Azides, *ACS Chem. Biol.*, 2006, **1**, 644–648.

69 A. Bernardin, A. Cazet, L. Guyon, P. Delannoy, F. Vinet, D. Bonnaffé and I. Texier, Copper-free click chemistry for highly luminescent quantum dot conjugates: Application to in vivo metabolic imaging, *Bioconjugate Chem.*, 2010, **21**, 583–588.

70 J. Dommerholt, S. Schmidt, R. Temming, L. J. A. Hendriks, F. P. J. T. Rutjes, J. C. M. van Hest, D. J. Lefeber, P. Friedl and F. L. van Delft, Readily Accessible Bicyclononynes for Bioorthogonal Labeling and Three-Dimensional Imaging of Living Cells, *Angew. Chem., Int. Ed.*, 2010, **49**, 9422–9425.

71 X. Ning, J. Guo, M. A. Wolfert and G.-J. Boons, Visualizing Metabolically Labeled Glycoconjugates of Living Cells by Copper-Free and Fast Huisgen Cycloadditions, *Angew. Chem., Int. Ed.*, 2008, **47**, 2253–2255.

72 M. F. Debets, S. S. van Berkel, S. Schoffelen, F. P. J. T. Rutjes, J. C. M. van Hest and F. L. van Delft, Aza-dibenzocyclooctynes for fast and efficient enzyme PEGylation *via* copper-free (3+2) cycloaddition, *Chem. Commun.*, 2010, **46**, 97–99.

73 N. E. Mbua, J. Guo, M. A. Wolfert, R. Steet and G.-J. Boons, Strain-Promoted Alkyne-Azide Cycloadditions (SPAAC) Reveal New Features of Glycoconjugate Biosynthesis, *ChemBioChem*, 2011, **12**, 1912–1921.

74 O. K. Arriortua, M. Insausti, L. Lezama, I. Gil, D. Muro, E. Garaio, J. Martínez, D. Fuente, R. M. Fratila, M. P. Morales, R. Costa, M. Eceiza, M. Sagartzazu-aizpurua and J. M. Aizpurua, Colloids and Surfaces B : Biointerfaces RGD-Functionalized Fe 3 O 4 nanoparticles for magnetic hyperthermia, *Colloids Surf., B*, 2018, **165**, 315–324.

75 R. Martínez, E. Polo, S. Barbosa, P. Taboada, P. del Pino and B. Pelaz, 808 nm-activable core@multishell upconverting nanoparticles with enhanced stability for efficient photodynamic therapy, *J. Nanobiotechnol.*, 2020, **18**, 85.

76 L. Du, H. Qin, T. Ma, T. Zhang and D. Xing, Vivo Imaging-Guided Photothermal/Photoacoustic Synergistic Therapy with Bioorthogonal Metabolic Glycoengineering-Activated Tumor Targeting Nanoparticles, *ACS Nano*, 2017, **11**, 8930–8943.

77 M. L. Blackman, M. Royzen and J. M. Fox, Tetrazine Ligation: Fast Bioconjugation Based on Inverse-Electron-Demand Diels–Alder Reactivity, *J. Am. Chem. Soc.*, 2008, **130**, 13518–13519.

78 N. K. Devaraj, R. Weissleder and S. A. Hilderbrand, Tetrazine-Based Cycloadditions: Application to Pretargeted Live Cell Imaging, *Bioconjugate Chem.*, 2008, **19**, 2297–2299.

79 A. Rondon and F. Degoul, Antibody Pretargeting Based on Bioorthogonal Click Chemistry for Cancer Imaging and Targeted Radionuclide Therapy, *Bioconjugate Chem.*, 2020, **31**, 159–173.

80 H. Wu and N. K. Devaraj, Advances in Tetrazine Bioorthogonal Chemistry Driven by the Synthesis of Novel Tetrazines and Dienophiles, *Acc. Chem. Res.*, 2018, **51**, 1249–1259.

81 M. R. Karver, R. Weissleder and S. A. Hilderbrand, Synthesis and Evaluation of a Series of 1,2,4,5-Tetrazines for Bioorthogonal Conjugation, *Bioconjugate Chem.*, 2011, **22**, 2263–2270.

82 Z. Hao, S. Hong, X. Chen and P. R. Chen, Introducing Bioorthogonal Functionalities into Proteins in Living Cells, *Acc. Chem. Res.*, 2011, **44**, 742–751.

83 K. Lang and J. W. Chin, Bioorthogonal Reactions for Labeling Proteins, *ACS Chem. Biol.*, 2014, **9**, 16–20.

84 K. L. Kiick, E. Saxon, D. A. Tirrell and C. R. Bertozzi, Incorporation of azides into recombinant proteins for chemoselective modification by the Staudinger ligation, *Proc. Natl. Acad. Sci.*, 2002, **99**, 19–24.

85 D. C. Dieterich, A. J. Link, J. Graumann, D. A. Tirrell and E. M. Schuman, Selective identification of newly synthesized proteins in mammalian cells using bioorthogonal noncanonical amino acid tagging (BONCAT), *Proc. Natl. Acad. Sci. U. S. A.*, 2006, **103**, 9482–9487.

86 M. Amiram, A. D. Haimovich, C. Fan, Y.-S. Wang, I. Ntai, D. W. Moonan, N. J. Ma, A. J. Rovner, S. Hoon, N. L. Kelleher, A. L. Goodman, M. C. Jewett, D. Söll, J. Rinehart and F. J. Isaacs, Evolution of translation components in recoded organisms enables multi-site nonstandard amino acid incorporation in proteins at high yield and purity, *Nat. Biotechnol.*, 2015, **33**, 1272–1278.

87 E. Saxon, S. J. Luchansky, H. C. Hang, C. Yu, S. C. Lee and C. R. Bertozzi, Investigating cellular metabolism of synthetic azidosugars with the Staudinger ligation, *J. Am. Chem. Soc.*, 2002, **124**, 14893–14902.

88 J. A. Prescher, D. H. Dube and C. R. Bertozzi, Chemical remodelling of cell surfaces in living animals, *Nature*, 2004, **430**, 873–878.

89 D. J. Vocadlo, H. C. Hang, E.-J. Kim, J. A. Hanover and C. R. Bertozzi, A chemical approach for identifying O-GlcNAc-modified proteins in cells, *Proc. Natl. Acad. Sci.*, 2003, **100**, 9116–9121.

90 H. C. Hang, C. Yu, D. L. Kato and C. R. Bertozzi, A metabolic labeling approach toward proteomic analysis of mucin-type O-linked glycosylation, *Proc. Natl. Acad. Sci. U. S. A.*, 2003, **100**, 14846–14851.

91 S. Hapuarachchige, W. Zhu, Y. Kato and D. Artemov, Bioorthogonal, two-component delivery systems based on antibody and drug-loaded nanocarriers for enhanced internalization of nanotherapeutics, *Biomaterials*, 2014, **35**, 2346–2354.

92 F.-J. Hsieh, S. Sotoma, H.-H. Lin, C.-Y. Cheng, T.-Y. Yu, C.-L. Hsieh, C.-H. Lin and H.-C. Chang, Bioorthogonal Fluorescent Nanodiamonds for Continuous Long-Term Imaging and Tracking of Membrane Proteins, ACS Appl. Mater. Interfaces, 2019, 11, 19774–19781.

93 C. Wu, Y. Jin, T. Schneider, D. R. Burnham, P. B. Smith and D. T. Chiu, Ultrabright and bioorthogonal labeling of cellular targets using semiconducting polymer dots and click chemistry, Angew. Chem., Int. Ed., 2010, 49, 9436–9440.

94 Y. Han, H. Pan, W. Li, Z. Chen, A. Ma, T. Yin, R. Liang, F. Chen, Y. Ma, Y. Jin, M. Zheng, B. Li and L. Cai, T Cell Membrane Mimicking Nanoparticles with Bioorthogonal Targeting and Immune Recognition for Enhanced Photothermal Therapy, Adv. Sci., 2019, 1900251.

95 J. B. Haun, N. K. Devaraj, S. A. Hilderbrand, H. Lee and R. Weissleder, Bioorthogonal chemistry amplifies nanoparticle binding and enhances the sensitivity of cell detection, Nat. Nanotechnol., 2010, 5, 660–665.

96 J. B. Haun, N. K. Devaraj, B. S. Marinelli, H. Lee and R. Weissleder, Probing intracellular biomarkers and mediators of cell activation using nanosensors and bioorthogonal chemistry, ACS Nano, 2011, 5, 3204–3213.

97 V. M. Peterson, C. M. Castro, H. Lee and R. Weissleder, Orthogonal Amplification of Nanoparticles for Improved Diagnostic Sensing, ACS Nano, 2012, 6, 3506–3513.

98 S. Hapuarachchige, Y. Kato and D. Artemov, Bioorthogonal two-component drug delivery in HER2(+) breast cancer mouse models, Sci. Rep., 2016, 6, 24298.

99 S. H. Lee, O. K. Park, J. Kim, K. Shin, C. G. Pack, K. Kim, G. Ko, N. Lee, S.-H. Kwon and T. Hyeon, Deep Tumor Penetration of Drug-Loaded Nanoparticles by Click Reaction-Assisted Immune Cell Targeting Strategy, J. Am. Chem. Soc., 2019, 141, 13829–13840.

100 S. Hapuarachchige, C. T. Huang, M. C. Donnelly, C. Bařinka, S. E. Lupold, M. G. Pomper and D. Artemov, Cellular Delivery of Bioorthogonal Pretargeting Therapeutics in PSMA-Positive Prostate Cancer, Mol. Pharm., 2020, 17, 98–108.

101 Z. Li, Z. Liu, Z. Chen, E. Ju, W. Li, J. Ren and X. Qu, Bioorthogonal chemistry for selective recognition, separation and killing bacteria over mammalian cells, Chem. Commun., 2016, 52, 3482–3485.

102 M. X. Gao, L. Yang, Y. Zheng, X. X. Yang, H. Y. Zou, J. Han, Z. X. Liu, Y. F. Li and C. Z. Huang, "Click" on Alkynylated Carbon Quantum Dots: An Efficient Surface Functionalization for Specific Biosensing and Bioimaging, Chem.–Eur. J., 2017, 23, 2171–2178.

103 N. Guldris, J. Gallo, L. García-Hevia, J. Rivas, M. Bañobre-López and L. M. Salonen, Orthogonal Clickable Iron Oxide Nanoparticle Platform for Targeting, Imaging, and On-Demand Release, Chem.–Eur. J., 2018, 24, 8624–8631.

104 H. Pan, P. Zhang, D. Gao, Y. Zhang, P. Li, L. Liu, C. Wang, H. Wang, Y. Ma and L. Cai, Noninvasive Visualization of Respiratory Viral Infection Using Bioorthogonal Conjugated Near-Infrared-Emitting Quantum Dots, ACS Nano, 2014, 8, 5468–5477.

105 H. Koo, S. Lee, J. H. Na, S. H. Kim, S. K. Hahn, K. Choi, I. C. Kwon, S. Y. Jeong and K. Kim, Bioorthogonal copper-free click chemistry inVivo for tumor-targeted delivery of nanoparticles, Angew. Chem., Int. Ed., 2012, 51, 11836–11840.

106 S. B. Lee, H. L. Kim, H. J. Jeong, S. T. Lim, M. H. Sohn and D. W. Kim, Mesoporous silica nanoparticle pretargeting for PET imaging based on a rapid bioorthogonal reaction in a living body, Angew. Chem, Int. Ed., 2013, 52, 10549–10552.

107 J. Gallo, N. Kamaly, I. Lavdas, E. Stevens, Q. De Nguyen, M. Wylezinska-Arridge, E. O. Aboagye and N. J. Long, CXCR4-targeted and MMP-responsive iron oxide nanoparticles for enhanced magnetic resonance imaging, Angew. Chem., Int. Ed., 2014, 53, 9550–9554.

108 S. Lee, H. Koo, J. H. Na, S. J. Han, H. S. Min, S. J. Lee, S. K. Kim, S. H. Yun, S. Y. Jeong, I. C. Kwon, K. Choi and K. Kim, Chemical Tumor-Targeting of Nanoparticles Based on Metabolic Glycoengineering and Click Chemistry, ACS Nano, 2014, 8, 2048–2063.

109 H. Y. Yoon, M. L. Shin, M. K. Shim, S. Lee, J. H. Na, H. Koo, H. Lee, J. H. Kim, K. Y. Lee, K. Kim and I. C. Kwon, Artificial Chemical Reporter Targeting Strategy Using Bioorthogonal Click Reaction for Improving Active-Targeting Efficiency of Tumor, Mol. Pharm., 2017, 14, 1558–1570.

110 T. Ito, T. Nakamura, E. Kusaka, R. Kurihara and K. Tanabe, Controlling localization and excretion of nanoparticles by click modification of the surface chemical structures inside living cells, Chempluschem, 2015, 80, 796–799.

111 R. Liu, J. Zhao, G. Han, T. Zhao, R. Zhang, B. Liu, Z. Liu, C. Zhang, L. Yang and Z. Zhang, Click-Functionalized SERS Nanoprobes with Improved Labeling Efficiency and Capability for Cancer Cell Imaging, ACS Appl. Mater. Interfaces, 2017, 9, 38222–38229.

112 S. Lee, S. Jung, H. Koo, J. H. Na, H. Y. Yoon, M. K. Shim, J. Park, J. H. Kim, S. Lee, M. G. Pomper, I. C. Kwon, C. H. Ahn and K. Kim, Nano-sized metabolic precursors for heterogeneous tumor-targeting strategy using bioorthogonal click chemistry in vivo, Biomaterials, 2017, 148, 1–15.

113 K. M. Au, A. Tripathy, C. P.-I. Lin, K. Wagner, S. Hong, A. Z. Wang and S. I. Park, Bespoke Pretargeted Nanoradioimmunotherapy for the Treatment of Non-Hodgkin Lymphoma, ACS Nano, 2018, 12, 1544–1563.

114 G. Lv, K. Li, L. Qiu, Y. Peng, X. Zhao, X. Li and Q. Liu, Enhanced Tumor Diagnostic and Therapeutic Effect of Mesoporous Silica Nanoparticle-Mediated Pre-targeted Strategy, Pharm. Res., 2018, 35, 63.

115 S. Lim, H. Y. Yoon, H. J. Jang, S. Song, W. Kim, J. Park, K. E. Lee, S. Jeon, S. Lee, D.-K. Lim, B.-S. Kim, D.-E. Kim and K. Kim, Dual-Modal Imaging-Guided Precise Tracking of Bioorthogonally Labeled Mesenchymal Stem Cells in Mouse Brain Stroke, ACS Nano, 2019, 13, 10991–11007.

116 H.-S. Han, E. Niemeyer, Y. Huang, W. S. Kamoun, J. D. Martin, J. Bhaumik, Y. Chen, S. Roberge, J. Cui, M. R. Martin, D. Fukumura, R. K. Jain, M. G. Bawendi and D. G. Duda, Quantum dot/antibody conjugates for in

vivo cytometric imaging in mice, *Proc. Natl. Acad. Sci.*, 2015, **112**, 1350–1355.

117 J. B. Haun, C. M. Castro, R. Wang, V. M. Peterson, B. S. Marinelli, H. Lee and R. Weissleder, Micro-NMR for Rapid Molecular Analysis of Human Tumor Samples, *Sci. Transl. Med.*, 2011, **3**, 71ra16.

118 M. Liong, M. Fernandez-Suarez, D. Issadore, C. Min, C. Tassa, T. Reiner, S. M. Fortune, M. Toner, H. Lee and R. Weissleder, Specific Pathogen Detection Using Bioorthogonal Chemistry and Diagnostic Magnetic Resonance, *Bioconjugate Chem.*, 2011, **22**, 2390–2394.

119 D. Issadore, J. Chung, H. Shao, M. Liong, A. A. Ghazani, C. M. Castro, R. Weissleder and H. Lee, Ultrasensitive Clinical Enumeration of Rare Cells ex Vivo Using a Micro-Hall Detector, *Sci. Transl. Med.*, 2012, **4**, 141ra92.

120 H. Shao, J. Chung, L. Balaj, A. Charest, D. D. Bigner, B. S. Carter, F. H. Hochberg, X. O. Breakefield, R. Weissleder and H. Lee, Protein typing of circulating microvesicles allows real-time monitoring of glioblastoma therapy, *Nat. Med.*, 2012, **18**, 1835–1840.

121 S. S. Agasti, R. H. Kohler, M. Liong, V. M. Peterson, H. Lee and R. Weissleder, Dual Imaging and Photoactivated Nanoprobe for Controlled Cell Tracking, *Small*, 2013, **9**, 222–227.

122 N. M. Robertson, Y. Yang, I. Khan, V. E. LaMantia, M. Royzen and M. V. Yigit, Single-trigger dual-responsive nanoparticles for controllable and sequential prodrug activation, *Nanoscale*, 2017, **9**, 10020–10030.

123 F. Emmetiere, C. Irwin, N. T. Viola-Villegas, V. Longo, S. M. Cheal, P. Zanzonico, N. Pillarsetty, W. A. Weber, J. S. Lewis and T. Reiner, 18 F-Labeled-Bioorthogonal Liposomes for In Vivo Targeting, *Bioconjugate Chem.*, 2013, **24**, 1784–1789.

124 G. Lu, F. Li, F. Zhang, L.-L. Huang, L. Zhang, Y. Lv, W. Wei and H.-Y. Xie, Amplifying Nanoparticle Targeting Performance to Tumor *via* Diels-Alder Cycloaddition, *Adv. Funct. Mater.*, 2018, **28**, 1707596.

125 S. Hou, J. S. Choi, M. A. Garcia, Y. Xing, K. J. Chen, Y. M. Chen, Z. K. Jiang, T. Ro, L. Wu, D. B. Stout, J. S. Tomlinson, H. Wang, K. Chen, H. R. Tseng and W. Y. Lin, Pretargeted positron emission tomography imaging that employs supramolecular nanoparticles with in vivo bioorthogonal chemistry, *ACS Nano*, 2016, **10**, 1417–1424.

126 O. Keinänen, E. M. Mäkilä, R. Lindgren, H. Virtanen, H. Liljenbäck, V. Oikonen, M. Sarparanta, C. Molthoff, A. D. Windhorst, A. Roivainen, J. J. Salonen and A. J. Airaksinen, Pretargeted PET Imaging of trans-Cyclooctene-Modified Porous Silicon Nanoparticles, *ACS Omega*, 2017, **2**, 62–69.

127 J. Pellico, I. Fernández-Barahona, M. Benito, Á. Gaitán-Simón, L. Gutiérrez, J. Ruiz-Cabello and F. Herranz, Unambiguous detection of atherosclerosis using bioorthogonal nanomaterials, *Nanomedicine*, 2019, **17**, 26–35.

128 J. M. Adrover, J. Pellico, I. Fernández-Barahona, S. Martín-Salamanca, J. Ruiz-Cabello, A. Hidalgo and F. Herranz,

129 Y. Feng, Y. Wu, J. Zuo, L. Tu, I. Que, Y. Chang, L. J. Cruz, A. Chan and H. Zhang, Assembly of upconversion nanophotosensitizer in vivo to achieve scatheless real-time imaging and selective photodynamic therapy, *Biomaterials*, 2019, **201**, 33–41.

Thrombo-tag, an in vivo formed nanotracer for the detection of thrombi in mice by fast pre-targeted molecular imaging, *Nanoscale*, 2020, **12**, 22978–22987.

130 X. Xie, B. Li, J. Wang, C. Zhan, Y. Huang, F. Zeng and S. Wu, Tetrazine-Mediated Bioorthogonal System for Prodrug Activation, Photothermal Therapy, and Optoacoustic Imaging, *ACS Appl. Mater. Interfaces*, 2019, **11**, 41875–41888.

131 J. A. C. M. Goos, M. Davydova, T. R. Dilling, A. Cho, M. A. Cornejo, A. Gupta, W. S. Price, S. Puttick, M. R. Whittaker, J. F. Quinn, T. P. Davis and J. S. Lewis, Design and preclinical evaluation of nanostars for the passive pretargeting of tumor tissue, *Nucl. Med. Biol.*, 2020, **84–85**, 63–72.

132 H. Li, J. Conde, A. Guerreiro and G. J. L. Bernardes, Tetrazine Carbon Nanotubes for Pretargeted In Vivo "Click-to-Release" Bioorthogonal Tumour Imaging, *Angew. Chem., Int. Ed.*, 2020, **59**, 16023–16032.

133 L. Zuo, J. Ding, C. Li, F. Lin, P. R. Chen, P. Wang, G. Lu, J. Zhang, L.-L. Huang and H.-Y. Xie, Coordinating bioorthogonal reactions with two tumor-microenvironment-responsive nanovehicles for spatiotemporally controlled prodrug activation, *Chem. Sci.*, 2020, **11**, 2155–2160.

134 E. J. L. Stéen, J. T. Jørgensen, K. Johann, K. Nørregaard, B. Sohr, D. Svatunek, A. Birke, V. Shalgunov, P. E. Edem, R. Rossin, C. Seidl, F. Schmid, M. S. Robillard, J. L. Kristensen, H. Mikula, M. Barz, A. Kjær and M. M. Herth, Trans -Cyclooctene-Functionalized PeptoBrushes with Improved Reaction Kinetics of the Tetrazine Ligation for Pretargeted Nuclear Imaging, *ACS Nano*, 2020, **14**, 568–584.

135 L. Tang, Q. Yin, Y. Xu, Q. Zhou, K. Cai, J. Yen, L. W. Dobrucki and J. Cheng, Bioorthogonal oxime ligation mediated in vivo cancer targeting, *Chem. Sci.*, 2015, **6**, 2182–2186.

136 P. J. O'Brien, S. Elahipanah, D. Rogozhnikov and M. N. Yousaf, Bio-Orthogonal Mediated Nucleic Acid Transfection of Cells *via* Cell Surface Engineering, *ACS Cent. Sci.*, 2017, **3**, 489–500.

137 K. Porte, B. Renoux, E. Péraudeau, J. Clarhaut, B. Eddhif, P. Poinot, E. Gravel, E. Doris, A. Wijkhuisen, D. Audisio, S. Papot and F. Taran, Controlled Release of a Micelle Payload *via* Sequential Enzymatic and Bioorthogonal Reactions in Living Systems, *Angew. Chem., Int. Ed.*, 2019, **58**, 6366–6370.

138 T. Terai and T. Nagano, Fluorescent probes for bioimaging applications, *Curr. Opin. Chem. Biol.*, 2008, **12**, 515–521.

139 J. Wiedenmann, F. Oswald and G. U. Nienhaus, Fluorescent proteins for live cell imaging: Opportunities, limitations, and challenges, *IUBMB Life*, 2009, **61**, 1029–1042.

140 K. Thorn, Genetically encoded fluorescent tags, *Mol. Biol. Cell*, 2017, **28**, 848–857.

141 V. Dunsing, M. Luckner, B. Zühlke, R. A. Petazzi, A. Herrmann and S. Chiantia, Optimal fluorescent protein tags for quantifying protein oligomerization in living cells, *Sci. Rep.*, 2018, **8**, 10634.

142 N. C. Shaner, G. H. Patterson and M. W. Davidson, Advances in fluorescent protein technology, *J. Cell Sci.*, 2007, **120**, 4247–4260.

143 A. R. Kherlopian, T. Song, Q. Duan, M. A. Neimark, M. J. Po, J. K. Gohagan and A. F. Laine, A review of imaging techniques for systems biology, *BMC Syst. Biol.*, 2008, **2**, 74.

144 M. Wu and J. Shu, Multimodal Molecular Imaging: Current Status and Future Directions, *Contrast Media Mol. Imaging*, 2018, **2018**, 1–12.

145 D. Jin, P. Xi, B. Wang, L. Zhang, J. Enderlein and A. M. van Oijen, Nanoparticles for super-resolution microscopy and single-molecule tracking, *Nat. Methods*, 2018, **15**, 415–423.

146 P. Sharma, S. Brown, G. Walter, S. Santra and B. Moudgil, Nanoparticles for bioimaging, *Adv. Colloid Interface Sci.*, 2006, **123–126**, 471–485.

147 Y. Chen and Z. Rosenzweig, Luminescent CdS Quantum Dots as Selective Ion Probes, *Anal. Chem.*, 2002, **74**, 5132–5138.

148 R. Hardman, A Toxicologic Review of Quantum Dots: Toxicity Depends on Physicochemical and Environmental Factors, *Environ. Health Perspect.*, 2006, **114**, 165–172.

149 C. Wu and D. T. Chiu, Highly Fluorescent Semiconducting Polymer Dots for Biology and Medicine, *Angew. Chem., Int. Ed.*, 2013, **52**, 3086–3109.

150 K. J. Mintz, Y. Zhou and R. M. Leblanc, Recent development of carbon quantum dots regarding their optical properties, photoluminescence mechanism, and core structure, *Nanoscale*, 2019, **11**, 4634–4652.

151 S. Y. Lim, W. Shen and Z. Gao, Carbon quantum dots and their applications, *Chem. Soc. Rev.*, 2015, **44**, 362–381.

152 S. Skylaki, O. Hilsenbeck and T. Schroeder, Challenges in long-term imaging and quantification of single-cell dynamics, *Nat. Biotechnol.*, 2016, **34**, 1137–1144.

153 V. N. Mochalin, O. Shenderova, D. Ho and Y. Gogotsi, The properties and applications of nanodiamonds, *Nat. Nanotechnol.*, 2012, **7**, 11–23.

154 S. Pilot, Durante, Orian, Bhamidipati and Fabris, A Review on Surface-Enhanced Raman Scattering, *Biosensors*, 2019, **9**, 57.

155 A.-I. Henry, B. Sharma, M. F. Cardinal, D. Kurouski and R. P. Van Duyne, Surface-Enhanced Raman Spectroscopy Biosensing: In Vivo Diagnostics and Multimodal Imaging, *Anal. Chem.*, 2016, **88**, 6638–6647.

156 M. A. Busquets, J. Estelrich and M. J. Sánchez-Martín, Nanoparticles in magnetic resonance imaging: from simple to dual contrast agents, *Int. J. Nanomed.*, 2015, 1727.

157 R. S. Mahla, Stem Cells Applications in Regenerative Medicine and Disease Therapeutics, *Int. J. Cell Biol.*, 2016, **2016**, 1–24.

158 M. R. Javan, A. Khosrojerdi and S. M. Moazzeni, New Insights Into Implementation of Mesenchymal Stem Cells in Cancer Therapy: Prospects for Anti-angiogenesis Treatment, *Front. Oncol.*, 2019, **9**, 840.

159 L. Accomasso, C. Gallina, V. Turinetto and C. Giachino, Stem Cell Tracking with Nanoparticles for Regenerative Medicine Purposes: An Overview, *Stem Cells Int.*, 2016, **2016**, 1–23.

160 X. Liu, Z. Yang, J. Sun, T. Ma, F. Hua and Z. Shen, A brief review of cytotoxicity of nanoparticles on mesenchymal stem cells in regenerative medicine, *Int. J. Nanomed.*, 2019, **14**, 3875–3892.

161 M. Patra, K. Zarschler, H.-J. Pietzsch, H. Stephan and G. Gasser, New insights into the pretargeting approach to image and treat tumours, *Chem. Soc. Rev.*, 2016, **45**, 6415–6431.

162 S. O. Kelley, What Are Clinically Relevant Levels of Cellular and Biomolecular Analytes?, *ACS Sens.*, 2017, **2**, 193–197.

163 Y. Wu, R. D. Tilley and J. J. Gooding, Challenges and Solutions in Developing Ultrasensitive Biosensors, *J. Am. Chem. Soc.*, 2019, **141**, 1162–1170.

164 L. Gloag, M. Mehdipour, D. Chen, R. D. Tilley and J. J. Gooding, Advances in the Application of Magnetic Nanoparticles for Sensing, *Adv. Mater.*, 2019, **31**, 1904385.

165 I. Gessner, J. W. U. Fries, V. Brune and S. Mathur, Magnetic nanoparticle-based amplification of microRNA detection in body fluids for early disease diagnosis, *J. Mater. Chem. B*, 2021, **9**, 9–22.

166 Z. Wang, P. Li, L. Cui, J.-G. Qiu, B. Jiang and C. Zhang, Integration of nanomaterials with nucleic acid amplification approaches for biosensing, *TrAC, Trends Anal. Chem.*, 2020, **129**, 115959.

167 J. Shi, P. W. Kantoff, R. Wooster and O. C. Farokhzad, Cancer nanomedicine: progress, challenges and opportunities, *Nat. Rev. Cancer*, 2017, **17**, 20–37.

168 C. Faustino, P. Rijo and C. P. Reis, Nanotechnological strategies for nerve growth factor delivery: Therapeutic implications in Alzheimer's disease, *Pharmacol. Res.*, 2017, **120**, 68–87.

169 M. Overchuk and G. Zheng, Overcoming obstacles in the tumor microenvironment: Recent advancements in nanoparticle delivery for cancer theranostics, *Biomaterials*, 2018, **156**, 217–237.

170 B. Baig, S. A. Halim, A. Farrukh, Y. Greish and A. Amin, Current status of nanomaterial-based treatment for hepatocellular carcinoma, *Biomed. Pharmacother.*, 2019, **116**, 108852.

171 N. Puttappa, R. S. Kumar, G. Kuppusamy and A. Radhakrishnan, Nano-facilitated drug delivery strategies in the treatment of plasmodium infection, *Acta Trop.*, 2019, **195**, 103–114.

172 J. Kim, S. I. Ahn and Y. Kim, Nanotherapeutics engineered to cross the blood-brain barrier for advanced drug delivery to the central nervous system, *J. Ind. Eng. Chem.*, 2019, **73**, 8–18.

173 T. A. Denison and Y. H. Bae, Tumor heterogeneity and its implication for drug delivery, *J. Controlled Release*, 2012, **164**, 187–191.

174 J. A. Prescher, D. H. Dube and C. R. Bertozzi, Chemical remodelling of cell surfaces in living animals, *Nature*, 2004, **430**, 873–877.

175 J. T. Weiss, J. C. Dawson, K. G. Macleod, W. Rybski, C. Fraser, C. Torres-Sánchez, E. E. Patton, M. Bradley, N. O. Carragher and A. Unciti-Broceta, Extracellular palladium-catalysed dealkylation of 5-fluoro-1-propargyl-uracil as a bioorthogonally activated prodrug approach, *Nat. Commun.*, 2014, **5**, 3277.

176 J. Clavadetscher, E. Indrigo, S. V. Chankeshwara, A. Lilienkampf and M. Bradley, In-Cell Dual Drug Synthesis by Cancer-Targeting Palladium Catalysts, *Angew. Chem., Int. Ed.*, 2017, **56**, 6864–6868.

177 M. A. Miller, B. Askevold, H. Mikula, R. H. Kohler, D. Pirovich and R. Weissleder, Nano-palladium is a cellular catalyst for in vivo chemistry, *Nat. Commun.*, 2017, **8**, 15906.

178 C. Ren, H. Liu, F. Lv, W. Zhao, S. Gao, X. Yang, Y. Jin, Y. Tan, J. Zhang, X.-J. Liang and Z. Li, Prodrug-Based Nanoreactors with Tumor-Specific In Situ Activation for Multisynergistic Cancer Therapy, *ACS Appl. Mater. Interfaces*, 2020, **12**, 34667–34677.

179 A. M. Pérez-López, B. Rubio-Ruiz, T. Valero, R. Contreras-Montoya, L. Álvarez de Cienfuegos, V. Sebastián, J. Santamaría and A. Unciti-Broceta, Bioorthogonal Uncaging of Cytotoxic Paclitaxel through Pd Nanosheet–Hydrogel Frameworks, *J. Med. Chem.*, 2020, **63**, 9650–9659.

180 T. T. V. Phan, T.-C. Huynh, P. Manivasagan, S. Mondal and J. Oh, An Up-To-Date Review on Biomedical Applications of Palladium Nanoparticles, *Nanomaterials*, 2019, **10**, 66.

181 M. A. Miller, H. Mikula, G. Luthria, R. Li, S. Kronister, M. Prytyskach, R. H. Kohler, T. Mitchison and R. Weissleder, Modular Nanoparticulate Prodrug Design Enables Efficient Treatment of Solid Tumors Using Bioorthogonal Activation, *ACS Nano*, 2018, **12**, 12814–12826.

182 M. Hoop, A. S. Ribeiro, D. Rösch, P. Weinand, N. Mendes, F. Mushtaq, X.-Z. Chen, Y. Shen, C. F. Pujante, J. Puigmartí-Luis, J. Paredes, B. J. Nelson, A. P. Pêgo and S. Pané, Mobile Magnetic Nanocatalysts for Bioorthogonal Targeted Cancer Therapy, *Adv. Funct. Mater.*, 2018, **28**, 1705920.

183 J. Li and P. R. Chen, Development and application of bond cleavage reactions in bioorthogonal chemistry, *Nat. Chem. Biol.*, 2016, **12**, 129–137.

184 S. Davies, B. J. Stenton and G. J. L. Bernardes, Bioorthogonal Decaging Reactions for Targeted Drug Activation, *Chim. Int. J. Chem.*, 2018, **72**, 771–776.

185 X. Ji, Z. Pan, B. Yu, L. K. De La Cruz, Y. Zheng, B. Ke and B. Wang, Click and release: bioorthogonal approaches to "on-demand" activation of prodrugs, *Chem. Soc. Rev.*, 2019, **48**, 1077–1094.

186 D. M. Patterson and J. A. Prescher, Orthogonal bioorthogonal chemistries, *Curr. Opin. Chem. Biol.*, 2015, **28**, 141–149.

187 N. K. Devaraj, The Future of Bioorthogonal Chemistry, *ACS Cent Sci*, 2018, **4**, 952–959.

188 W. Luo, J. Luo, V. V. Popik and M. S. Workentin, Dual-Bioorthogonal Molecular Tool: "Click-to-Release" and "Double-Click" Reactivity on Small Molecules and Material Surfaces, *Bioconjugate Chem.*, 2019, **30**, 1140–1149.